

1 **Earth Orbit v2.1: a 3D Visualization and**  
2 **Analysis Model of Earth's Orbit,**  
3 **Milankovitch Cycles and Insolation**

4  
5 **Tihomir Sabinov Kostadinov<sup>1,2</sup> and Roy Gilb<sup>1</sup>**

6 [1] Department of Geography and the Environment, 28 Westhampton Way, University of  
7 Richmond, Richmond, VA 23173, USA

8 [2] Formerly at Earth Research Institute, University of California Santa Barbara, Santa  
9 Barbara, CA 93106, USA

10  
11 Correspondence to: T. S. Kostadinov (tkostadi@richmond.edu)

12  
13  
14  
15  
16 T.S. Kostadinov dedicates this paper to his Mother, who first sparked his interest in the  
17 magnificent night sky and the science of astronomy.

18  
19  
20  
21  
22 Version 2 – revised after reviewer comments

23 March 25, 2014

24

1 **Abstract**

2 Milankovitch theory postulates that periodic variability of Earth's orbital elements is a major  
3 climate forcing mechanism, causing, for example, the contemporary glacial-interglacial  
4 cycles. There are three Milankovitch orbital parameters: orbital eccentricity, precession and  
5 obliquity. The interaction of the amplitudes, periods and phases of these parameters controls  
6 the spatio-temporal patterns of incoming solar radiation (insolation) and the timing of the  
7 seasons with respect to perihelion. This complexity makes Earth-Sun geometry and  
8 Milankovitch theory difficult to teach effectively. Here, we present "Earth Orbit v2.1": an  
9 astronomically precise and accurate model that offers 3D visualizations of Earth's orbital  
10 geometry, Milankovitch parameters and the ensuing insolation forcing. The model is  
11 developed in MATLAB® as a user-friendly graphical user interface. Users are presented  
12 with a choice between the Berger (1978a) and Laskar et al. (2004) astronomical solutions for  
13 eccentricity, obliquity and precession. A "demo" mode is also available, which allows the  
14 Milankovitch parameters to be varied independently of each other, so that users can isolate  
15 the effects of each parameter on orbital geometry, the seasons, and insolation. A 3D orbital  
16 configuration plot, as well as various surface and line plots of insolation and insolation  
17 anomalies on various time and space scales are produced. Insolation computations use the  
18 model's own orbital geometry with no additional *a-priori* input other than the Milankovitch  
19 parameter solutions. Insolation output and the underlying solar declination computation are  
20 successfully validated against the results of Laskar et al. (2004) and Meeus (1998),  
21 respectively. The model outputs some ancillary parameters as well, e.g. Earth's radius-vector  
22 length, solar declination and day length for the chosen date and latitude. Time-series plots of  
23 the Milankovitch parameters and several relevant paleoclimatological data sets can be  
24 produced. Both research and pedagogical applications are envisioned for the model.

25  
26  
27  
28  
29

## 1 **1 Introduction**

2 The astrophysical characteristics of our star, the Sun, determine to first order the continuously  
3 habitable zone around it (Kasting et al., 1993; Kasting, 2010), in which rocky planets are able  
4 to maintain liquid water on their surface and sustain life. The surface temperature of a planet  
5 depends to first order upon the incoming flux of solar radiation (insolation) to its surface.  
6 Additionally, energy for our metabolism (and most of modern economy) is obtained  
7 exclusively from the Sun via the process of oxygenic photosynthesis performed by green  
8 terrestrial plants and marine phytoplankton. The high oxygen content of Earth's atmosphere,  
9 necessary for the evolution of placental mammals (Falkowski et al., 2005), is due to billions  
10 of years of photosynthesis and the geological burial of reduced carbon equivalents (Falkowski  
11 et al., 2008a; Falkowski et al., 2008b; Kump et al., 2010). Thus, the Sun is central to climate  
12 formation and stability and to our evolution and continued existence as a species.

13

14 The temporal and spatial patterns of insolation and their variability on various scales  
15 determine climatic stability over geologic time, as well as climate characteristics such as  
16 diurnal, seasonal and pole to Equator temperature contrasts, all of which influence planetary  
17 habitability. Insolation can change due to changes in the luminosity of the Sun itself. This  
18 can happen due to the slow increase of solar luminosity that gives rise to the Faint Young Sun  
19 Paradox (Kasting, 2010; Kump et al., 2010), or it can happen on much shorter time scales  
20 such as the 11-yr sunspot cycle (Fröhlich, 2013; Hansen et al., 2013). Importantly, insolation  
21 is also affected by the orbital elements of the planet. According to the astronomical theory of  
22 climate, quasi-periodic variations in Earth's orbital elements cause multi-millennial variability  
23 in the spatio-temporal distributions of insolation, and thus provide an external forcing and  
24 pacing to Earth's climate (Milankovitch, 1941; Berger 1988; Berger and Loutre, 1994; Berger  
25 et al., 2005). These periodic orbital fluctuations are called Milankovitch cycles, after the  
26 Serbian mathematician Milutin Milanković who was instrumental in developing the theory  
27 (Milankovitch, 1941). Laskar et al. (2004) provide a brief historical overview of the main  
28 contributions leading to the pioneering work of Milanković. There are three Milankovitch  
29 orbital parameters: orbital eccentricity (main periodicities of ~100 and 400 kyr (1 kyr = one  
30 thousand years)), precession (quantified as the longitude of perihelion relative to the moving  
31 vernal equinox, main periodicities ~19 and 23 kyr) and obliquity of the ecliptic (main  
32 periodicity 41 kyr) (Berger 1978a). Obliquity is strictly speaking a rotational, rather than an

1 orbital parameter; however, we refer to it here either as an orbital or Milankovitch parameter,  
2 for brevity.

3

4 The pioneering work by Hays et al. (1976) demonstrated a strong correlation between these  
5 cycles and paleoclimatological records. Since then, multiple analyses of paleoclimate records  
6 have been found to be consistent with Milankovitch forcing (e.g. Imbrie et al., 1992; Rial,  
7 1999; Lisiecki and Raymo, 2005). Notably, the glacial-interglacial cycles of the Quaternary  
8 have been strongly linked to orbital forcing, particularly summertime insolation at high  
9 Northern latitudes (Milankovitch, 1941; Berger 1988; Berger and Loutre, 1994; Bradley, 2014  
10 and refs. therein). Predicting the Earth system response to orbital forcing (including glacier  
11 growth and melting) is not trivial, and there are challenges in determining which insolation  
12 quantity (i.e. integrated over what time and space scales) is responsible for paleoclimate  
13 change, e.g. peak summer insolation intensity, or overall summertime integrated insolation at  
14 Northern latitudes (Imbrie et al., 1993; Lisiecki et al., 2008; Huybers, 2006; Huybers and  
15 Denton, 2008; Bradley, 2014). Moreover, some controversies related to the astronomical  
16 theory remain, notably the 100-kyr problem, or the so-called mid-Pleistocene transition. This  
17 refers the fact that the geological record indicates that the last 1,000 kyr have been dominated  
18 by 100-kyr glacial-interglacial cycles, a gradual switch from the previously dominant 41-kyr  
19 periodicity. This transition cannot be explained by orbital forcing alone, as there was actually  
20 a decrease in 100-kyr variance in this eccentricity band (e.g. Imbrie et al., 1993; Loutre et  
21 al., 2004; Berger et al., 2005; Bradley 2014 and refs. therein). Current consensus focuses on  
22 the explanation that the mid-Pleistocene transition is due to factors within the Earth system  
23 itself, rather than astronomical factors – e.g. internal climate system oscillations, nonlinear  
24 responses due to the continental ice sheet size, or CO<sub>2</sub> degassing from the Southern Ocean  
25 (Bradley 2014, Sect. 6.3.3 and 6.3.4 and refs. therein) Finally, alternative astronomical  
26 influences on climate have also been proposed, such as the influence of the orbital  
27 inclination cycle (Muller and McDonald, 1997).

28

29 The Milankovitch cycles are due to complex gravitational interactions between the bodies of  
30 the solar system. Astronomical solutions for the values of the Milankovitch orbital  
31 parameters have been derived by Berger (1978a) and Berger (1978b), referred to henceforth  
32 as Be78 (valid for 1,000 kyr before and after present), and Laskar et al. (2004), referred to

1 henceforth as La2004 (valid for 101,000 kyr before present to 21,000 kyr after present). Here  
2 the present is defined as the start of Julian epoch 2000 (J2000), i.e. the Gregorian calendar  
3 date of January 1, 2000 at 12:00 UT (universal time, formerly known as Greenwich Mean  
4 Time)). There are several other solutions as well, e.g. Berger and Loutre (1992) and Laskar et  
5 al. (2011). These astronomical solutions are crucial for paleoclimate and climate science, as  
6 they enable the computation of insolation at any latitude and time period in the past or future  
7 within the years spanned by the solutions (Berger and Loutre, 1994, Berger et al. 2010,  
8 Laskar et al., 2004), and subsequently the use of this insolation in climate models as forcing  
9 (e.g. Berger et al., 1998). Climate models are an important method for testing the response of  
10 the Earth system to Milankovitch forcing.

11

12 While most Earth science students and professionals are well aware of Earth's orbital  
13 configuration and the basics of the Milankovitch cycles, the details of both and the way the  
14 Milankovitch orbital elements influence spatio-temporal patterns of insolation on various time  
15 and space scales remain elusive. It is difficult to appreciate the pivotal importance of  
16 Kepler's laws of planetary motion in controlling the effects of Milankovitch cycles on  
17 insolation patterns. The three-dimensional nature of Earth's orbit, the vast range of space and  
18 time scales involved, and the geometric details are complex, and yet those same factors  
19 present themselves to computer modeling and 3D visualization. Here, we present "Earth  
20 Orbit v2.1": an astronomically precise and accurate 3-D visualization and analysis model of  
21 Earth's orbit, Milankovitch cycles, and insolation. The model is envisioned for both research  
22 and pedagogical applications and offers 3D visualizations of Earth's orbital geometry,  
23 Milankovitch parameters and the ensuing insolation forcing. It is developed in MATLAB®  
24 and has an intuitive, user-friendly graphical user interface (GUI) (Fig. 1). Users are presented  
25 with a choice between the Be78 and La2004 astronomical solutions for eccentricity, obliquity  
26 and precession. A "demo" mode is also available, which allows the three Milankovitch  
27 parameters to be varied independently of each other (and exaggerated over much larger ranges  
28 than the naturally occurring ones), so users can isolate the effects of each parameter on orbital  
29 geometry, the seasons, and insolation. Users select a calendar date and the Earth is placed in  
30 its orbit using Kepler's laws; the calendar can be started on either vernal equinox (March 20)  
31 or perihelion (Jan. 3). A 3D orbital configuration visualization, as well as spatio-temporal  
32 surface and line plots of insolation and insolation anomalies (with respect to J2000) on

1 various scales are then produced. Below, we first describe the model parameters and  
2 implementation. We then detail the model user interface, provide instructions on its  
3 capabilities and use, and describe the output. We then present successful model validation  
4 results, which are comparisons to existing independently derived insolation, solar declination  
5 and season length values. Finally, we conclude with brief analysis of sources of uncertainty.  
6 Throughout, we provide examples of the pedagogical value of the model.

7  
8 Various insolation solutions and visualizations exist (Berger, 1978a; Rubincam, 1994  
9 (however, see response of Berger, 1996); Laskar et al., 2004; Archer, 2013; Huybers, 2006).  
10 Notably, the AnalySeries software (Paillard et al., 1996; Paillard, 2014) shares many of the  
11 functionalities presented here and offers many additional ones, such as paleoclimatic time-  
12 series analysis and many more choices for insolation computation. Importantly, the model  
13 presented here was developed independently from AnalySeries (or other similar efforts) and  
14 computes insolation from first principles of orbital mechanics (Kepler's laws) and irradiance  
15 propagation, using exclusively its own internal geometry. The only model inputs are the three  
16 Milankovitch orbital parameters, either real astronomical solutions (Be78 or La2004) or user-  
17 entered demo values. No insolation computation code from the above-cited existing solutions  
18 has been used, so comparison with these solutions constitutes independent model verification,  
19 referred to here as validation, because we consider the La2004 and Meeus (1998) solutions  
20 the geophysical truth (Sect. 5).

21  
22 The unique contribution of our model consists of the *combination* of the following features: a)  
23 central to the whole model is a user-controllable, 3D pan-tilt-zoom plot of the actual Earth  
24 orbit, b) an interactive user-friendly GUI that serves as a single-entry control panel for the  
25 entire model and makes it suitable for use by non-programmers and friendly to didactic  
26 applications, c) the Milankovitch cycles are incorporated explicitly and insolation is output  
27 according to real or user-selected demo orbital elements, which d) allows users to enter  
28 exaggerated orbital parameters independently of each other and isolate their effects on  
29 insolation, as well as view the orbit with exaggerated eccentricity e) the source code is  
30 published and advanced users can check its logic, as well as modify it and adapt it, and f) the  
31 software is platform-independent.

32

1 The issue of climate change has come to the forefront of Earth science and policy and it is  
2 arguably the most important global issue of immediate and long-term consequences (e.g.  
3 IPCC, 2013). Earth's climate varies naturally over multiple time scales, from decadal to  
4 hundreds of millions of years (e.g. Kump et al., 2010). It is thus crucial to understand natural  
5 climate forcings, their time scales, and the ensuing response of the Earth system. In addition,  
6 detailed understanding of the Sun's daily path in the sky and the patterns of insolation have  
7 become important to increasing numbers of students and professionals because of the rise in  
8 usage of solar power (thermal and photovoltaic). We submit that the model presented here  
9 can enhance understanding of all of these important subject areas.

10

## 11 **2 Key Definitions, Model Parameters and Implementation**

12 The model input parameters, and their values and units, are summarized in Table 1. The  
13 following definitions, discussion and symbols are consistent with those of Berger et al.  
14 (2010). The reader is referred to their Figure 1. According to Kepler's First Law of Planetary  
15 Motion, Earth's orbit is an ellipse, and the Sun is in one of its foci (e.g. Meeus, 1998). Orbital  
16 eccentricity,  $e$  (Table 1), is a measure of the deviation of Earth's orbital ellipse from a circle  
17 and is defined as  $e = \sqrt{1 - b^2 / a^2}$ , where  $a$  is the semi-major axis (Table 1) and  $b$  is the semi-  
18 minor axis of the orbital ellipse (e.g. Berger and Loutre, 1994). The semi-major axis is about  
19 equal to 1 AU (Meeus, 1998; Standish et al., 1992) and determines the size of the orbital  
20 ellipse and thus the orbital period of Earth; it is considered a fixed constant in the model, as  
21 its variations are extremely small (Berger et al, 2010; Laskar et al, 2004, their Fig. 11).  
22 Various orbital period definitions are possible; here, the sidereal period is used as a model  
23 constant (Meeus, 1998). Thus, Kepler's Third Law of Planetary Motion is implicit in these  
24 two constant definitions and is not included explicitly elsewhere in model logic. The  
25 obliquity of Earth,  $\epsilon$ , is the angle between the direction of its axis of rotation and the normal  
26 to the orbital plane, or the ecliptic (Table 1). Eccentricity and obliquity are two of the three  
27 Milankovitch orbital parameters.

28

29 The third Milankovitch orbital parameter, precession, is the most challenging for instruction  
30 and visualization. There are two separate kinds of precession that combine to create a  
31 climatic effect – precession of the equinoxes (also termed axial precession), and apsidal

1 precession, i.e. precession of the perihelion in the case of Earth's orbit. Axial precession  
2 refers to the wobbling of Earth's axis of rotation that slowly changes its absolute orientation  
3 in space with respect to the distant stars. The axis of rotation describes a cone (one in each  
4 hemisphere) in space with a periodicity of about 26,000 years (Berger and Loutre, 1994).  
5 This is the reason why the star  $\alpha$  UMi (present-day Polaris, or the North Star), has not and  
6 will not always be aligned with the direction of the North Pole. Also, due to axial precession,  
7 the point of vernal equinox in the sky moves with respect to the distant stars and occurs in  
8 successively earlier zodiacal constellations. Axial precession is clockwise as viewed from  
9 above the North Pole, hence the North Celestial Pole describes a counter-clockwise motion as  
10 viewed by an observer looking in the direction of the North Ecliptic Pole. Precession of the  
11 perihelion refers to the gradual rotation of the line joining aphelion and perihelion, with  
12 respect to the distant stars (or the reference equinox of a given epoch) (Berger, 1978a, Berger  
13 and Loutre, 1994).

14

15 Axial precession and precession of the perihelion combine to modulate the *relative* position of  
16 the equinoxes and solstices (i.e. the seasons) with respect to perihelion, which is what is  
17 relevant for insolation and climate. This climatically-relevant precession is implemented in  
18 the model and is quantified via the longitude of perihelion,  $\tilde{\omega}$ , which is the angle between the  
19 directions of the moving fall equinox and perihelion at a given time, measured  
20 counterclockwise in the plane of the ecliptic (Berger et al., 2010). Because both perihelion  
21 and equinox move, the longitude of perihelion will have a different (shorter) periodicity than  
22 one full cycle of axial wobbling alone (Berger and Loutre, 1994). The direction of Earth's  
23 radius-vector when Earth is at fall equinox (~Sept. 22) is referred to as the direction of fall  
24 equinox above. This is the direction with respect to the distant stars where the Sun would be  
25 found on its annual motion on the ecliptic on March 20<sup>th</sup> – i.e. at vernal equinox. In other  
26 words, that is the direction of the vernal point in the sky (Berger et al. 2010, their Fig. 1 &  
27 Appendix B), the origin of the right ascension coordinate. This distinction between vernal  
28 equinox and the direction of the vernal point can cause confusion, especially since the exact  
29 definition of longitude of perihelion can vary (e.g. c.f. Berger et al., 1978a; Berger et al.,  
30 1993; Berger and Loutre 1994; Jousaume and Braconnot, 2007; Berger et al., 2010) and the  
31 longitude of perihelion can also be confused with the longitude of perigee,  $\omega = \tilde{\omega} + 180^\circ$ ,  
32 which is the angle between the directions of vernal equinox and perihelion, measured

1 counterclockwise as viewed from the North Pole direction, in the plane of the orbit (Berger et  
2 al, 2010). Here, we use the terminology and definitions of Berger et al. (2010).

3

4 The magnitude of the climatic effect of precession is modulated by eccentricity. In the  
5 extreme example, if eccentricity were exactly zero, the effects of precession would be null.  
6 Climatic precession,  $e\sin\omega$ , is the parameter that quantifies precession and determines season  
7 lengths, the Earth-Sun distance at summer solstice (Berger and Loutre, 1994) and various  
8 important insolation quantities (Berger et al., 1993, their Table 1). This interplay between  
9 eccentricity and precession presents an important way to introduce both concepts  
10 pedagogically and to test student comprehension.

11

12 The solar “constant”,  $S_o$ , is defined here as the total solar irradiance (TSI) on a flat surface  
13 perpendicular to the solar rays at a reference distance of exactly 1 AU (Table 1). As Berger et  
14 al. (2010) note, due to eccentricity changes, the mean distance from the Earth to the Sun over  
15 a year is not constant on geologic time scales. It also matters how this mean distance is  
16 defined – e.g. over time (mean anomaly) vs. over angle (true anomaly). True and mean  
17 anomaly are defined below in Sect. 2.1 & 2.2, respectively. If  $S_o$  is defined to be the  
18 irradiance from the Sun at the mean Earth-Sun distance, then it is indeed not a true constant.  
19 As used here,  $S_o$  is a true model constant as long as the luminosity of the Sun itself is assumed  
20 constant. The default value is chosen to be  $1,366 \text{ W m}^{-2}$  (Fröhlich, 2013). Recent evidence  
21 suggests that the appropriate value may actually be about  $1,361 \text{ W m}^{-2}$  (Kopp and Lean,  
22 2011). Users can change the value of  $S_o$  independently of other model inputs in order to  
23 study the effects of changes in absolute solar luminosity – e.g. in order to simulate the Faint  
24 Young Sun (e.g. Kasting, 2010) or the sunspot cycle (e.g. Hansen, 2013).

25

## 26 **2.1 Model Coordinate System; Sun-Earth Geometry Parameterization; Solar** 27 **Declination**

28 According to Kepler’s First Law of Planetary Motion, Earth orbits the Sun in an ellipse, and  
29 the Sun is in one of the ellipse’s foci. The heliocentric equation of the orbital ellipse in polar  
30 form is given by (Meeus, 1998; his Eq. 30.3):

$$1 \quad |\mathbf{r}(v)| = \frac{a(1-e^2)}{1+e\cos v} \quad (1)$$

2 In the above, the Sun is at the origin of the coordinate system,  $a$  is the semi-major axis of the  
 3 orbital ellipse,  $e$  is eccentricity,  $v$  is true anomaly, and  $\mathbf{r}$  is Earth's instantaneous radius-vector,  
 4 i.e. the vector originating at the Sun and ending at the instantaneous planetary position. True  
 5 anomaly,  $v$ , is the angle between the directions of perihelion and the radius-vector, subtended  
 6 at the Sun and measured counter-clockwise in the plane of the orbit (e.g. Meeus (1998), his  
 7 Ch. 30; Berger et al. (2010) their Fig. 1). The true longitude of the Sun (or simply true  
 8 longitude) is equal to Earth's true anomaly plus the longitude of perigee (Berger et al., 2010,  
 9 their Eq. 6). True longitude is the angle Earth has swept from its orbit, subtended at the Sun,  
 10 since it was last at vernal equinox, and it is equivalent to the angle the Sun has travelled along  
 11 the ecliptic in the same time. Mean longitude is the longitude of the mean Sun, in an  
 12 imaginary perfectly circular orbit of the same period, i.e. mean longitude is proportional to the  
 13 passage of time, much like mean anomaly (See Sect. 2.2 below).

14

15 In the Earth Orbit v2.1 model, given a user-selected calendar date, true anomaly,  $v$ , is  
 16 determined by solving the inverse Kepler equation (see Section 2.2 below). The Earth's  
 17 radius vector is then solved for using Eq. 1 above. Because the main model coordinate  
 18 system is heliocentric Cartesian, the  $(\mathbf{r},v)$  pair of polar coordinates is then transformed to  
 19 Cartesian  $(x,y)$  for plotting. The Earth is initially parameterized as a sphere in its own  
 20 geocentric Cartesian coordinate system in terms of its radius and geographic latitude and  
 21 longitude (corresponding to the two angles of a spherical coordinate system). The Earth's  
 22 coordinate system's  $x$  and  $y$  axes are in the plane of the Equator (shown as a black dotted line,  
 23 Fig. 2), and its  $z$ -axis is pointing towards the true North Pole and is coinciding with Earth's  
 24 axis of rotation; these axes are also plotted in black dotted lines, the  $z$ -axis is lengthened  
 25 toward North so that it pierces Earth's surface and is labeled, since this is critical in the  
 26 definition and understanding of the seasons. Earth is plotted as a transparent mesh so that  
 27 important orbital elements can be seen through it at various zoom levels (Fig. 2). The color  
 28 scale of Earth's mesh is just a function of latitude and no day and night sides are explicitly  
 29 shown. Earth's radius is not to scale with the orbit itself or with the Sun's radius. Thus, the  
 30 center of Earth has its true geometric orbital position (and is the tip of its instantaneous  
 31 radius-vector); however the surface of the sphere in the model is arbitrary and must not be

1 interpreted as the true surface onto which insolation is computed, for example. The insolation  
2 computations (Sect. 2.3) are geocentric. The Sun is also plotted (not to scale) as a sphere  
3 centered at the origin of the main model coordinate system.

4  
5 The Earth is oriented properly in 3D with respect to the orbital ellipse by using a rotation  
6 matrix to rotate its coordinate system. The 3D rotation matrix is computed using Rodrigues'  
7 formula (Belongie, 2013) for 3D rotation about a given direction by a given angle. The  
8 direction about which Earth is rotated is determined by a vector which is always in the orbital  
9 plane ( $\mathbf{k}$ -component is zero), and the  $\mathbf{i}$  and  $\mathbf{j}$  components are determined by the longitude of  
10 perihelion. The angle by which Earth is rotated is determined by obliquity. Thus, the rotation  
11 matrix is a function of two of the three Milankovitch parameters and is a valuable and useful  
12 instructional tool/concept for lessons in geometry, mathematics, astronomy, physical  
13 geography, and climatology. At this point the Earth is correctly oriented in 3D space with  
14 respect to its orbit and the distant stars. Earth is then translated to its proper instantaneous  
15 position on its orbit by addition of its radius-vector to all relevant Earth-bound model  
16 elements (which are then plotted in the main heliocentric coordinate system).

17  
18 Declination is one of the two spherical coordinates of the equatorial astronomical coordinate  
19 system. It is measured along a celestial meridian (hour circle) and is defined as the angle  
20 between the celestial Equator and the direction toward the celestial object (Meeus, 1998).  
21 Solar declination varies with the seasons, due to obliquity. It is zero at the equinoxes, reaches  
22 a maximum of  $+\varepsilon$  at summer solstice and a minimum of  $-\varepsilon$  at winter solstice. Solar  
23 declination determines the length of day and the daily path of the Sun in the sky at a given  
24 latitude, i.e. its altitude and azimuth above the horizon as a function of time. Thus, solar  
25 declination determines instantaneous and time-integrated insolation. In turn, solar declination  
26 and its evolution over the course of a year are a function of the orbital elements; thus it  
27 provides the mathematical and conceptual link between the Milankovitch orbital elements and  
28 insolation and climate. Here, we compute instantaneous solar declination using the angle  
29 between the direction of the North Pole and Earth's radius-vector, calculated using their dot  
30 product. Thus, we explicitly compute solar declination from the geometry of the model and it  
31 is a model *emergent property* rather than prescribed *a-priori*; therefore, this also applies to  
32 insolation computations (Section 2.3 and Sect. 5).

1

## 2 **2.2 Implementation of Kepler’s Second Law of Planetary Motion**

3 The heliocentric position of a planet in an elliptical orbit at a given instant of time is given in  
4 terms of its true anomaly,  $\nu$  – see Eq. 1 and Section 2.1 above. True anomaly can also be  
5 thought of as the angle (subtended at the Sun) which the planet has “swept” from its orbit  
6 since last perihelion passage. Kepler’s Second Law of planetary motion states that the planet  
7 will “sweep” equal areas of its orbit in equal intervals of time and governs the value of true  
8 anomaly as a function of time (e.g. Meeus, 1998; Jousaume and Braconnot, 1997). At non-  
9 zero eccentricity,  $\nu$  is not simply proportional to time since last perihelion passage (time of  
10 flight) expressed as a fraction of the orbital period in angular units. The latter quantity is  
11 called mean anomaly,  $M$ . Kepler’s Second Law is used to relate  $M$  and  $\nu$ , using an auxiliary  
12 quantity called eccentric anomaly,  $E$ .  $E$  and  $M$  are related by Kepler’s Equation (Meeus,  
13 1998):

$$14 \quad E = M + e \sin E, \tag{2}$$

15 where  $e$  is orbital eccentricity. When  $E$  is known,  $\nu$  can be solved for using (Meeus, 1998):

$$16 \quad \tan \frac{\nu}{2} = \sqrt{\frac{1+e}{1-e}} \tan \frac{E}{2} \tag{3}$$

17 The forward Kepler problem consists of solving for time of flight,  $M$ , given the planetary  
18 position,  $\nu$ . This is straightforward by first solving for  $E$  in Eq. 3 and using it to solve for  $M$   
19 in Eq. 2.

20

21 However, in the most intuitive case, which is implemented here, the user enters a desired date,  
22 and the position of the planet has to be determined from the date, i.e. time of flight/mean  
23 anomaly  $M$  is given, and true anomaly has to be determined. This is referred to as the inverse  
24 Kepler problem and amounts to solving for  $E$  in Eq. 2 and then for  $\nu$  in Eq. 3. Solving for  $E$   
25 is not straightforward, as no analytical solution exists. Numerous numerical methods exist for  
26 the solution of the inverse Kepler problem. Here, the binary search algorithm of Sinnott et al.  
27 (1985) is used, as given in Meeus (1998). It has the advantage of being computationally  
28 efficient, which becomes important when time series of insolation is the desired model output.

1 It also has the distinct advantages of being valid for any value of eccentricity and converging  
2 to the exact solution to within the user machine's precision.

3

### 4 **2.3 Implementation of Insolation Computation**

5 Instantaneous insolation at the top of the atmosphere (TOA) can be computed as:

$$6 \quad S(h, \mathbf{r}) = S_o \left( \frac{|\mathbf{r}_o|}{|\mathbf{r}|} \right)^2 \sin h, \quad (4)$$

7 Where  $|\mathbf{r}|$  is the length of the radius-vector of Earth expressed in AU, and  $h$  is the altitude of  
8 the Sun above the horizon (e.g. Berger et al., 2010). Eq. 4 is an expression of the inverse  
9 square law and Lambert cosine law of irradiance. The radius-vector length is computed in the  
10 model for the chosen date (and not for every instant) using Eq. 1.  $S_o$  is the TSI at  $|\mathbf{r}_o| = 1$  AU  
11 by definition (Sect. 2). In this equation insolation,  $S$ , is defined as the total (spectrally  
12 integrated) solar radiant energy impinging at the TOA on a unit surface area parallel to the  
13 mathematical horizon at a given latitude at a given instant.  $S$  carries the units of  $S_o$ , here  $\text{W}$   
14  $\text{m}^{-2}$ .  $S$  needs to be integrated over time and/or space in order to compute insolation quantities  
15 of interest. Here, the main discrete time step over which  $S$  is computed and output is one 24-  
16 hour period, i.e. daily insolation.

17

18 Daily insolation is a function of latitude, date, and  $S_o$ . The date is associated with a given true  
19 anomaly for a given calendar start date and orbital configuration (Joussaume and Braconnot,  
20 1997; Sect. 2.3.1). This determines the current solar declination and the length of the radius-  
21 vector of Earth, i.e. the Sun-Earth distance. The user inputs the desired latitude, date and TSI,  
22 and the rest of the quantities are computed from the model geometry. Solar declination and  
23 the latitude determine the daily evolution of solar altitude,  $h$ , as a function of time, as follows  
24 (e.g. Meeus 1998):

$$25 \quad \sin h = \sin \delta \sin \phi + \cos \delta \cos \phi \cos t \quad (5)$$

26 In the above equation  $\delta$  is solar declination,  $\phi$  is geographic latitude on Earth, and  $t$  is the hour  
27 angle of the Sun.  $\delta$  is assumed constant for the day of interest, and  $t$  is a measure of the

1 progress of time. Half the day length,  $t_s$ , (i.e. the time between local solar noon and sunset), is  
2 determined by setting  $h = 0^\circ$  in Eq. 5:

$$3 \quad t_s = \text{acos}(-\tan \phi \tan \delta) \quad (6)$$

4 Eq. 5 is integrated over time from solar noon to sunset in order to compute the time-average  
5 of the sine of the solar altitude for the given date and latitude:

$$6 \quad \text{sinh\_ave} = \frac{1}{t_s} \int_0^{t_s} (\sin \delta \sin \phi + \cos \delta \cos \phi \cos t) dt \quad (7)$$

7 Eq. 7 is integrated numerically with a very small time step of about 10 s. Because the altitude  
8 of the Sun is symmetric about solar noon, it is sufficient to integrate only from solar noon to  
9 sunset time. Daily insolation is then computed by using the time-averaged *sinh\_ave* quantity  
10 in Eq. 4. The results are scaled by multiplying by the actual day length and dividing by 24  
11 hours. The resulting quantity represents the mean daily insolation over a full day, which is  
12 the standard value used in astronomical, climate and paleoclimate science (e.g. Laskar 2014).  
13 If this daily insolation is multiplied by 24 h (in seconds), total energy receipt for that day (in J  
14  $\text{m}^{-2}$ ) can be calculated.

15

16 At high latitudes, there are periods of the year with no sunset or no sunrise. These cases  
17 depend on the relationship of latitude and solar declination (e.g. Berger et al., 2010). They are  
18 handled separately by either integrating Eq. 7 over 24 hrs, or, in the case of no sunrise (polar  
19 night), assigning a value of exactly 0  $\text{W m}^{-2}$  to daily insolation.

20

### 21 2.3.1 Integrating Insolation over Longer Time Periods - Caveats

22 Because of the varying eccentricity and longitude of perihelion, there is no fixed  
23 correspondence between true anomaly and any one single calendar date, even if one were to  
24 define a fixed calendar start date. True anomaly and longitude are the astronomically rigorous  
25 ways to define a certain moment in Earth's year and seasons (e.g. Berger et al., 2010). If one  
26 wishes to make insolation comparisons between different orbital configurations, one must  
27 define strictly a calendar start date, and even then insolation will be in phase for different  
28 geological periods only for that date (Joussaume and Braconnot, 1997). Thus, the question  
29 "What is insolation on June 20?" is ill posed, unless one defines strictly what is meant by the

1 date of June 20. The problem persists if one wishes to compare insolation integrated over  
2 periods of time longer than a day, because over geologic time scales, absolute values and the  
3 interval of time true anomalies "swept" between two classical calendar dates are not constant.  
4 Thus, there are two ways to define a calendar – the classical or fixed-day calendar, in which  
5 month lengths follow the present-day configuration and the date of vernal equinox is fixed, or  
6 a fixed-angular calendar, which defines months beginning at certain true longitudes (function  
7 of true anomaly and the precession phase, see also Sect 4.2. below) and they can therefore  
8 have different number of days depending on the orbital configuration (Joussaume and  
9 Braconnot, 1997; Chen et al. 2010). The time intervals between solstices and equinoxes also  
10 varies, because of varying eccentricity and because these intervals happen in different places  
11 in the orbit with respect to perihelion. Thus season lengths vary over geologic time. Earth  
12 orbit v2.1 outputs season length in the main GUI to emphasize this important fact. Earth  
13 Orbit v2.1 uses the classical calendar dates (24 hr periods) as the user time input, rather than  
14 true anomaly or true longitude. This choice is much more intuitive to non-experts, and serves  
15 the educational purposes of the model best. The user has as a choice of calendar start date  
16 (Sect. 3) and true solar longitude is output (Sect. 4.2) to remind users of the above  
17 considerations. The effect of calendar choice on insolation phases and comparisons and on  
18 climate models is discussed at length by Joussaume and Braconnot (1997), Timm et al. (2008)  
19 and Chen et al. (2010).

20

21 The time step of integration can also influence the results of insolation computations, e.g. if  
22 annual insolation is averaged with a 5-day step, results are substantially different from the  
23 case when a 1-day step is used (not shown). For this reason, the model computes annually  
24 averaged insolation at a given latitude by using 1-day steps of integration. Finally, we note  
25 that the daily insolation computations of the model are robust and validated (Sect. 5.1);  
26 however, the model currently has limited functionality for making comparisons of insolation  
27 integrated over longer time periods over different geologic scales. In order to make such  
28 comparisons, the use of the elliptical integrals method of Berger et al. (2010) is  
29 recommended, as well as the Laskar et al. (2004) methods, both of which come with  
30 accompanying software (Laskar(2014) and Berger (2014), respectively). In addition, users  
31 are referred to the latest version of the AnalySeries software package (Paillard et al., 1996;

1 Paillard, 2014) for additional insolation and time series options. All of the above can also be  
2 used for verification of the output of the model presented here.

### 3 **3 Model User Interface**

4 The Earth orbit model is provided as supplementary material (Appendix A). The model is  
5 developed and runs in MATLAB®. All model control is realized via a single, user-friendly  
6 GUI panel (Fig. 1). Users are presented with a choice between the Be78 and the La2004  
7 astronomical solutions for eccentricity, obliquity and precession. A “demo” mode is also  
8 available. If a real astronomical solution is chosen, users are asked to input a year before or  
9 after present (defined as J2000, i.e. January 1, 2000 at 12 noon UT, see *Introduction*) for  
10 which they wish to run the model. The GUI only allows users to choose years within the  
11 respective solution’s validity: the Be78 solution is available for 1,000 kyr before and after  
12 present (J2000), whereas the La2004 solution is available for 101,000 kyr in the past and  
13 21,000 kyr in the future. The La2004 solutions are provided by Laskar (2014) (specifically at  
14 <http://www.imcce.fr/Equipes/ASD/insola/earth/La2004/index.html>) in tabulated form in 1 kyr  
15 intervals. The Be78 solutions are obtained by transcribing code from NASA GISS (see  
16 *Acknowledgements*). The model looks up the values of eccentricity, obliquity and precession  
17 for the chosen year and solution (using linear interpolation between tabulated years if  
18 necessary), and these values are used in subsequent visualizations and analyses. If the user  
19 chooses the “demo” mode, they select, independently of each other, the values of the  
20 Milankovitch parameters, which can be greatly exaggerated. In this way users can isolate the  
21 effects of each parameter on orbital geometry, the seasons, and insolation. The “demo” mode  
22 is central to the pedagogical value and applications of the model because it allows users to  
23 build and visualize an imaginary orbit of, for example, very high eccentricity while keeping  
24 obliquity fixed. Moreover, it will output all subsequent parameters, such as solar declination,  
25 day length, radius-vector length, based on this exaggerated imaginary orbit.

27  
28 Users input the desired calendar date, geographic latitude on Earth (positive degrees in the  
29 Northern Hemisphere and negative degrees in the Southern Hemisphere), and desired value of  
30 TSI. The calendar date defaults to the current date, latitude defaults to 43° N, and TSI  
31 defaults to 1,366 W m<sup>-2</sup> (Sect. 2). Two choices of calendar start date are available: either fix  
32 vernal equinox to be at the beginning of March 20<sup>th</sup> (default), or fix perihelion to be at the

1 beginning of Jan. 3<sup>rd</sup>. The availability of this choice complicates interpretation of model  
2 output; however it has high instructional value. It illustrates that the choice of calendar start  
3 date and a calendar system is a human construct, accepted by convention; it is based on the  
4 actual year and day length but is relative. This can also help test knowledge of the concepts  
5 explained in Sect. 2.3.1. The effect of the different choice of calendar start date is most  
6 apparent at exaggerated eccentricities and/or at longitudes of perihelion that are very different  
7 from the contemporary value. Insolation time series output (Sect. 4) is only computed for the  
8 calendar being fixed to vernal equinox on March 20<sup>th</sup>.

9

## 10 **4 Model Output**

### 11 **4.1 Graphical Output**

12 The main output of the model is a 3D plot of Earth's orbital configuration. Fig. 2A illustrates  
13 the orbital configuration using the contemporary values of the Milankovitch parameters (the  
14 La2004 solution for J2000 is shown), for September 16. The current phase of the precession  
15 cycle is such that Northern Hemisphere winter solstice occurs shortly before perihelion  
16 (longitude of perihelion is  $\sim 102.9^\circ$ ). This results in Northern hemisphere spring and summer  
17 being longer than the respective fall and winter (as shown in the GUI, Fig. 1). Fig 2B  
18 illustrates the orbital configuration also on Sept. 16 and using the La2004 solution, but for 10  
19 kyr in the future. Since this represents about a half of a precession cycle, the timing of the  
20 seasons is approximately  $180^\circ$  out of phase with respect to the contemporary configuration  
21 (the longitude of perihelion is  $\sim 279.2^\circ$ , and Northern hemisphere summer occurs near  
22 perihelion and is the shortest season). Because we chose to fix the calendar start date such  
23 that vernal equinox is always on March 20, and the eccentricity is fairly low, the date Sept. 16  
24 still occurs near the fall equinox, like in the contemporary example. However, because the  
25 length of time passing between vernal equinox and fall equinox is now shorter, Sept 16 almost  
26 coincides with fall equinox, unlike the contemporary case. Of course obliquity and  
27 eccentricity have also changed 10 kyr in the future, but unlike the longitude of perihelion,  
28 their changes are small in absolute terms, and thus this cannot be readily visualized by  
29 comparing Figs. 2A and 2B. This is one reason why it is very useful to have the ability to  
30 choose arbitrary independent value of the Milankovitch parameters in the demo mode,  
31 constructing an imaginary orbit. Fig. 2C illustrates one example of such an imaginary orbit

1 with greatly exaggerated eccentricity (0.6) and obliquity ( $45^\circ$ ) and longitude of perihelion of  
2  $225^\circ$ , i.e. very different from the J2000 values. This imaginary orbit illustrates that the date  
3 July 1 can occur in the Fall, due to the large eccentricity and the specific phase of precession  
4 chosen. Spring lasts only  $\sim 20$  days in this configuration because it occurs during perihelion  
5 passage, where the planet is much faster according to Kepler's Second Law, as compared to  
6 aphelion passage (Fall lasts  $\sim 229$  days in this configuration). Summer lasts about 58 days.  
7 Thus, July 1 occurs during the Fall season, counterintuitively. Importantly, such an  
8 exaggerated eccentricity means that the planet is very close to the Sun during perihelion, and  
9 some really high insolation values can occur even at modest solar declinations (e.g. for March  
10 29, at  $43^\circ\text{N}$ , solar declination is  $\sim 27^\circ$ , daylength is  $\sim 16$  hours, and daily insolation is  $3,307 \text{ W}$   
11  $\text{m}^{-2}$ , far exceeding any contemporary value anywhere on Earth). The reason is that the Sun-  
12 Earth distance then is only 0.4 AU, and the distance factor becomes a first-order effect on  
13 insolation, whereas it is a second-order factor in the real Earth orbit configuration (angle  
14 being the first-order factor, see Eq. 4).

15

16 The plots of Fig. 2 have pan-tilt-zoom capability, so users can view the orbital configuration  
17 from many perspectives; this is at the core of the pedagogical value of the model. The plot is  
18 updated with the current parameter selections by pressing the "Plot/Update Orbit" button.  
19 Finally, note that the orbits of Fig. 2 can be viewed from any angle and the apparent  
20 eccentricity of the orbits also changes with the view angle and the projection onto a 2D  
21 screen. This should not be confused with the intrinsic orbital eccentricity, which can be also  
22 judged by the relative distance of the orbital foci (marked with an 'x') from the ellipse's center  
23 (the intersection of the semi-major and semi-minor axes, red lines in Fig. 2)

24

25 Users are presented with several options of plotting insolation as function of time and latitude.  
26 First, insolation can be plotted for a single year (using the currently selected Milankovitch  
27 parameters) as a function of day of year and latitude (Fig. 3A, upper panel). Insolation  
28 anomalies with respect to the J2000 La2004 orbital configuration are also plotted, using  $S_o =$   
29  $1,366 \text{ W m}^{-2}$  (Fig. 3A, lower panel). Anomalies are especially useful when analyzing the  
30 effect of changes in insolation on the glacial-interglacial cycles. For example, the anomalies  
31 at  $65^\circ\text{N}$  during summer months 115 kyr before present (Fig. 3A, lower panel) suggest the  
32 inception of glaciation (e.g. Jousaume and Braconnot, 1997), as these areas were receiving

1 about 35-40 W m<sup>-2</sup> less insolation than they are receiving now. The data in these plots is  
2 computed with a step of 5 days and 5 degrees of latitude. Multi-millennial insolation time  
3 series can also be plotted in a 3D surface plot as a function of year since J2000 and day of  
4 year, at the selected latitude. Users select the start and end years for the time series. The data  
5 for these plots are computed for steps of 1 kyr and one day (for day of year). An example of  
6 the output is provided in Fig. 3B.

7

8 Several time series line plots are also produced. Insolation time series are plotted for the  
9 currently selected latitude; both the currently selected date and the annual average are shown  
10 (Fig. 4A). A multi-panel plot (Fig. 4B) allows the comparison of the three Milankovitch  
11 parameters. Precession is visualized as the longitude of perihelion, as well as the climatic  
12 precession parameter,  $esin\omega$  (Berger and Loutre, 1994). A separate GUI button allows users  
13 to optionally produce time series plots of several paleoclimatic data sets (Fig. 4C). The top  
14 panel shows the EPICA CO<sub>2</sub> (Lüthi et al., 2008a; Lüthi et al., 2008b) and deuterium  
15 temperature (Jouzel et al., 2007a; Jouzel et al., 2007b) time series which go back to ~800 kyr  
16 before present. The bottom panel of Fig. 4C shows two benthic oxygen isotope ( $\delta^{18}\text{O}$ ) data  
17 set compilations – the Lisiecki and Raymo (2005) benthic stack (Lisiecki, 2014) and the  
18 Zachos et al. (2001) data (Zachos et al., 2008). These data sets go back to 5,320 kyr and  
19 67,000 kyr before present, respectively. To first order, higher  $\delta^{18}\text{O}$  values are associated with  
20 higher continental ice sheet volumes and lower benthic ocean water temperatures (Zachos et  
21 al., 2001). For this reason, the y-axis of the lower panel of Fig. 4C is inverted, so that higher  
22 values of EPICA CO<sub>2</sub> and temperature (generally warmer climates) from the upper panel of  
23 Fig. 4C can be easily associated with lower  $\delta^{18}\text{O}$  values (also generally warmer climates).  
24 These paleoclimatic data are included for convenience of the user and no further interpretation  
25 or analyses are provided. Users are cautioned that the interpretation of these paleoclimatic  
26 signals and their uncertainties, time-resolution and chronology (age models) is fairly complex  
27 (e.g. Bradley, 2014 and data source references) and beyond the scope of this work. They are  
28 provided here for illustrative purposes only, e.g. it enables users to easily visualize the last  
29 few glacial-interglacial cycles (and the mid-Pleistocene transition to 100-kyr cyclicity, see  
30 *Introduction*), or to visually correlate these paleoclimatic time series with the corresponding  
31 Milankovitch parameter and insolation curves.

## 4.2 Numerical/Ancillary Output

Ancillary data (and their units) are output in the main GUI window (Fig. 1) and are updated every time the Earth orbit plot (Figs. 2) is re-drawn (Sect. 4.1), i.e. every time the "Plot/Update Orbit" button is pressed. Variables that are output in the main GUI are as follows: solar declination, insolation at the TOA for the chosen date and latitude, day length, Sun-Earth distance, length of the seasons (as defined in the North hemisphere (NH)), the longitude of perigee, and true and mean longitude of the Sun. As a reminder, the longitude of perigee is the angle between the directions of vernal equinox and perihelion and true longitude is the angle Earth has swept from its orbit, subtended at the Sun, since it was last at vernal equinox; mean longitude is proportional to time instead (for detailed definitions, see Sect 2 and 2.1 above). Users also are given the option of saving the data used to make the insolation plots in Fig. 3 in ASCII format. The first row and column of these files list the abscissa and ordinate values of the data, respectively.

## 5 Model Validation

### 5.1 Insolation Validation

Daily insolation is the most important model output from climate science perspective and is the fundamental discrete time unit at which the model calculates energy receipt at the TOA. Daily insolation was validated against the results of Laskar et al. (2004), as provided in Laskar (2014) (specifically, the pre-compiled Windows package at <http://www.imcce.fr/Equipes/ASD/insola/earth/binaries/index.html>). In both the Earth Orbit model and the Laskar software, the La2004 solution for the orbital parameters was used, and the default model solar constant (Table 1) was used. Laskar (2014) defines March 21 as vernal equinox, whereas Earth Orbit v2.1 fixes vernal equinox on March 20 for insolation time series. This was taken into account in this validation. Two dates were tested – March 21 and June 20 (according to the Earth Orbit v2.1 calendar; this corresponds to  $1^\circ$  and  $90^\circ$  mean longitude for the Laskar (2014) software), at three latitudes – 20 S, 45 N and 65 N. The entire time series from 200 kyr in the past to 200 kyr in the future (present = J2000) were tested with a time step of 1 kyr. Validation is excellent; virtually all test cases result in differences in insolation of less than  $1 \text{ W m}^{-2}$  for March 21 and less than  $2 \text{ W m}^{-2}$  for June 20, respectively (Fig. 5A and 5B, solid lines with dots), which corresponds to less than 0.5% of the absolute

1 values (Fig. 5C and 5D, solid lines with dots). Importantly, these differences are generally  
2 much smaller or of the same order of magnitude as the corresponding differences between the  
3 Be78 and La2004 astronomical solutions as computed by Earth Orbit v2.1 (Fig. 5, dashed  
4 lines). Furthermore, these differences are generally smaller than the uncertainty resulting  
5 from varying estimates of the TSI (e.g. Fröhlich 2013 vs. Kopp and Lean, 2011, see Sect. 2);  
6 also, these differences are smaller than the total contemporary anthropogenic radiative forcing  
7 on climate due to fossil fuel emissions (IPCC, 2013; their Fig. SPM. 5).

8  
9 The Earth Orbit v2.1 model uses its own internally constructed orbital geometry and first  
10 principles equations to compute insolation. There is no additional *a-priori* prescribed  
11 constraint to the model other than the orbital elements astronomical solution and the semi-  
12 major axis and orbital period (Sects. 2, 2.3; Table 1). Therefore the validation presented here  
13 is an independent verification of the model's geometry and computations, taking the Laskar  
14 (2014) values as truth. Sect. 6 discusses sources of model uncertainty which can explain  
15 some of the small differences observed.

## 16 **5.2 Solar Declination Validation and Season Length Validation**

17 Solar declination was validated against the algorithms of Meeus (1998). The model year is  
18 neither leap, nor common (Table 1) and is thus not equivalent to any single Gregorian  
19 calendar year. In order to validate declination at all dates, the Meeus (1998) algorithm was  
20 used to compute solar declinations for 12 UT on each date of four years (2009-2012, 2012  
21 being leap) and average the declinations for each date (not day of year, Fig. 6). These  
22 averages were then compared to the solar declination output by the model for that date.  
23 Results indicate differences are always less than  $\sim 0.2^\circ$  (Fig. 6, black line). By construction,  
24 model solar declination on March 20<sup>th</sup> will always be exactly zero degrees. In reality, the  
25 exact instance of vernal equinox varies year to year, so these validation differences are  
26 expected. Importantly, the differences between the model and the 4-yr averaged Meeus  
27 (1998) declinations are consistently smaller than the daily rate of change of declination (Fig.  
28 6, green curve), as computed from the Meeus (1998) data. Additionally, these differences are  
29 of a similar magnitude to the standard deviation of declination between these four years for  
30 each date (Fig. 6, red curve). Thus the solar declination validation is excellent and model  
31 configuration for each date is representative of a typical generic Gregorian calendar date. The

1 discontinuities in the Meeus (1998)–derived curves in Fig 6 (red and green) are due to  
2 omitting Feb 29, 2012 when averaging declination values for each date. The discontinuities  
3 in the Earth Orbit v2.1 to Meeus (1998) comparison curve (Fig. 6, black curve) are due to the  
4 above, plus the fact that the length of the model year is equal to the sidereal orbital period and  
5 thus March 19 is a longer "day" in the model year, since calendar start is fixed as vernal  
6 equinox on March 20 (also see Sect. 6 below). Finally, season lengths are an excellent method  
7 to validate the geometry of the model, because they test that the model is correctly computing  
8 a given time of flight on the orbit for a section of the orbit that corresponds to a given season,  
9 and generally not coinciding with special points such as perihelion. Season lengths agree to  
10 within 0.01 days with the tabulated values of Meeus (1998) (his Table 27F).

11

## 12 **6 Sources of Uncertainties**

13 Assumptions and approximations in the model and the underlying astronomical solutions  
14 propagate to uncertainties in the model outputs, such as declination and insolation. Some of  
15 these assumptions were already discussed, such as calculating insolation for a given calendar  
16 date vs. true anomaly interval (fixed-date vs fixed-angle calendars), and choosing integration  
17 steps for insolation time series (Sect. 2.3.1). The calendar bias discussed in detail in Sect.  
18 2.3.1 means that if one compares insolation over geologic time on a given classical calendar  
19 date, e.g. Sept. 16, which occurs a given number of 24-h periods after the fixed vernal  
20 equinox, one is not necessarily comparing insolation at the same true longitude. The same  
21 argument is valid for an arbitrary interval of time longer than a day and shorter than a full  
22 orbital cycle. This calendar bias creates the artificial North-South tilt observed in insolation  
23 anomalies (Chen et al., 2010), which is also exhibited by the Earth Orbit v2.1 model output  
24 (Fig. 3A, second panel). This is expected because Earth Orbit v2.1 uses the classical calendar  
25 dates, which are more user-friendly.

26

27 Next, we draw the users' attention to a few additional sources of uncertainty. Determination  
28 of some of these uncertainties is outside the scope of this work; however, users can run  
29 sensitivity analyses using the model in order to quantify them. Importantly, uncertainties in  
30 the astronomical solutions that are used as input to the model will propagate to insolation  
31 computations. There are differences between the different astronomical solutions (e.g. Fig.  
32 5). Accuracy is highest near the present time and degrades further into the past or future

1 (Laskar, 1999; Laskar et al, 2004). Chaotic components of planetary orbital motions  
2 introduce an uncertainty that increases by an order of magnitude every ten million years,  
3 making it impossible to obtain astronomical solutions for the Milankovitch parameters over  
4 period longer than a few tens of millions of years (Laskar et al., 2004). As a reminder, the  
5 Be78 solution is valid for one million years in the past or future, whereas the La2004 solution  
6 is valid from 101 million years before present to 21 million years in the future; however,  
7 solutions for times further back in time than 50 million years before present should be treated  
8 with caution (Laskar et al., 2004)..

9

10 Due to the gravitational interaction of Earth and other solar system bodies, in particular  
11 Jupiter, Venus and the Moon, high frequency variability (time scales of years to centuries) of  
12 the Milankovitch parameters is superimposed on the long-term low-frequency Milankovitch  
13 cycles. An example of such variability is the nutation in obliquity with a period of ~18 yr.  
14 These high frequency fluctuations also lead to insolation changes. Bertrand et al. (2002) used  
15 results from the VSOP82 planetary position solution (Bretagnon, 1982) and a simple climate  
16 model to demonstrate that the amplitudes of these high-frequency variations and the effect on  
17 insolation and surface temperature is negligible (equivalent to model noise) as compared to  
18 the 11-yr Sun cycle or the low-frequency trends.

19

20 The model is prescribed the sidereal year as the orbital period (Table 1), which is slightly  
21 longer than the tropical year (Meeus, 1998). The difference is of the order of 0.01 days. The  
22 use of these two different period definitions leads to negligible differences in solar declination  
23 on a given date (not shown), much smaller than the validation differences of Fig. 6. We  
24 conclude that the choice of orbital period does not influence the insolation computations  
25 significantly.

26

27 A single value for solar declination and the radius-vector length is used in the computation of  
28 daily insolation (Sect. 2.3). In reality, these quantities change continuously, instead of having  
29 discrete values. This is likely to introduce small errors in insolation that will be smaller in  
30 magnitude than the difference in daily insolation between successive days. Sunrise and sunset  
31 times used in the insolation computation are referred to the center of the disk of the Sun and

1 the mathematical horizon at the given latitude at the surface of Earth. Note also that  
2 irradiance is given at the top of the atmosphere (TOA), but all computations are geocentric,  
3 rather than topocentric, which should lead to negligible insolation differences.

4

5 Since the model year is not an integral number of days, if total annual insolation is computed  
6 by summing daily insolation values, the March 19 insolation needs to be scaled by 1.256363  
7 to reflect the fact that this day is  $24 \times 1.256363$  hrs long in the model (Berger et al. 2010).  
8 Here, we average daily insolation to output average annual insolation, so this correction is not  
9 applied.

10

## 11 **7 Concluding Remarks**

12 We presented Earth Orbit v2.1, an interactive 3D analysis and visualization model of the  
13 Earth orbit, Milankovitch cycles, and insolation. The model is written and runs in  
14 MATLAB® and is controlled from a single integrated user-friendly GUI. Users choose a real  
15 astronomical solution for the Milankovitch parameters or user-selected demo values. The  
16 model outputs a 3D plot of Earth's orbital configuration (with pan-tilt-zoom capability),  
17 selected insolation time series, and numerical ancillary data. The model is intended for both  
18 research and educational use. We emphasize the pedagogical value of the model and envision  
19 some of its primary uses will be in the classroom. The user-friendly GUI makes the model  
20 very accessible to non-programmers. It is also accessible to non-experts and the primary and  
21 secondary education classroom, as minimal scientific background is required to use the model  
22 in an instructional setting. Disciplines for which the model can be used span mathematics  
23 (e.g. spherical geometry, linear algebra, curve and surface parameterizations), astronomy,  
24 computer science, geology, Earth system science, climatology and paleoclimatology, physical  
25 geography and related fields.

26

27 The authors encourage feedback and request that comments, suggestions, and reports of  
28 errors/omissions be directed to [tkostadi@richmond.edu](mailto:tkostadi@richmond.edu)

29

## 30 **Appendix A: Code Availability & License**

1 The files necessary to run the model "Earth Orbit v2.1" in MATLAB® are provided here as  
2 Supplement. In addition, model files are expected to be available on the website of the  
3 University of Richmond Department of Geography and the Environment  
4 (<http://geography.richmond.edu>), under the *Resources* category; documented updates may be  
5 posted there. Sources of external data files are properly acknowledged in the file header  
6 and/or the ReadMe.txt file, as well as in this manuscript. The GUI is raised by typing the  
7 name of the associated script ('Earth\_orbit\_v2\_1.m') on the MATLAB® command line. The  
8 model has been tested in MATLAB® release R2013b on 64-bit Windows 7 Enterprise SP1  
9 and Linux Ubuntu 12.04 LTS, but should run correctly in earlier versions of MATLAB® and  
10 on different platforms. The model is distributed under the Creative Commons BY-NC-SA 3.0  
11 license. It is free for use, distribution and modification for non-commercial purposes. Details  
12 are provided in the ReadMe.txt file.

13

14 Supplementary material related to this article is available online at [\[To copy editor: Link here\]](#)

15

## 16 **Acknowledgements**

17 Funding for this work was provided to T. S. Kostadinov by the Andrew W. Mellon  
18 Foundation/Associated Colleges of the South Environmental Postdoctoral Fellowship and the  
19 University of Richmond School of Arts & Sciences. The University of Richmond School of  
20 Arts & Sciences also provided funding for R. Gilb. We would especially like to acknowledge  
21 Dr. Martin Medina for his help and the incredibly inspirational discussions. This project  
22 would not have been conceived without him. We also thank André Berger and Jacques  
23 Laskar for their Milankovitch and insolation solutions and software, Jacques Laskar for  
24 providing input data files for his solutions, and Gary L. Russell/NASA GISS for the Berger  
25 Milankovitch solutions FORTRAN® code. We thank David Kitchen, Jon Giorgini and  
26 William Folkner for the useful discussions. Oxygen isotope data compilations (LR04 and  
27 Zachos et al. 2001) and EPICA data sets authors and contributors are also hereby  
28 acknowledged. T.S Kostadinov expresses his gratitude to Dr. Van Nall and Dr. Della  
29 Dumbaugh for their multivariate calculus and linear algebra classes at University of  
30 Richmond, as well as to other mathematics and computer science faculty at the University of  
31 Richmond. We thank Jean Meeus for his excellent *Astronomical Algorithms*. T.S.  
32 Kostadinov thanks his astronomy teacher, Ms. Vanya Angelova, for being instrumental in

1 developing his interests in astronomy. We also thank the Wikipedia® Project and its  
2 contributors for providing multiple articles on mathematics, astronomy, orbital mechanics,  
3 and Earth Science that are a great first step in conducting research. We thank two anonymous  
4 reviewers for providing constructive comments that improved this manuscript.  
5

1 **References**

2 Archer, D (2013), Orbital Forcing of Climate,  
3 <http://forecast.uchicago.edu/Projects/orbits.doc.html>, last accessed September 24, 2013.

4

5 Belongie, Serge (2013), "Rodrigues' Rotation Formula." From *MathWorld* - A Wolfram Web  
6 Resource, created by Eric W. Weisstein.  
7 <http://mathworld.wolfram.com/RodriguesRotationFormula.html>, last accessed September 12,  
8 2013.

9

10 Berger, A.L. (1978a), Long-term variations of daily insolation and Quaternary climatic  
11 changes, *J Atmos Sci*, 35: 2362-2367

12

13 Berger, André L. (1978b), A Simple Algorithm to Compute Long Term Variations of Daily  
14 Insolation, Institut D'Astronomie et de Géophysique, Université Catholique de Louvain,  
15 Louvain-la Neuve, No. 18.

16

17 Berger, A. (1988), Milankovitch theory and climate. *Reviews of geophysics*, 26(4), 624-657.

18

19 Berger, A., & Loutre, M. F. (1992). Astronomical solutions for paleoclimate studies over the  
20 last 3 million years. *Earth and Planetary Science Letters*, 111(2), 369-382.

21

22 Berger, A., Loutre, M. F., & Tricot, C, (1993). Insolation and Earth's orbital periods. *Journal*  
23 *of Geophysical Research*, 98(D6), 10341-10362.

24

25 Berger, A. and M.F. Loutre (1994), Precession, eccentricity, obliquity, insolation and  
26 paleoclimates, In: "Long Term Climatic Variations, Data and Modelling", J.Cl. Duplessy and  
27 M.T. Spyridakis (Eds), NATO ASI Series, vol. 22, pp. 107-151, Springer-Verlag Berlin  
28 Heidelberg.

1

2 Berger, A. (1996), Comments to “Insolation in terms of Earth's orbital parameters” by DP  
3 Rubincam—Theor. Appl. Climatol. 48, 195–202, 1994. *Theoretical and applied climatology*,  
4 53(4), 253-255.

5

6 Berger A., M.F. Loutre, and H. Gallee, (1998), Sensitivity of the LLN climate model to the  
7 astronomical and CO<sub>2</sub> forcings over the last 200 kyr, *Climate Dynamics*, 14, pp. 615-629.

8

9 Berger, A., J. L. Mélice, and M. F. Loutre (2005), On the origin of the 100-kyr cycles in the  
10 astronomical forcing, *Paleoceanography*, 20, PA4019, doi:10.1029/2005PA001173.

11

12 Berger, A, Marie-France Loutre, Qiuzhen Yin (2010), Total irradiation during any time  
13 interval of the year using elliptic integrals, *Quaternary Science Reviews* 29 (2010) 1968-1982.

14

15 Berger, A (2014), <ftp://ftp.elic.ucl.ac.be/berger/ellipt/>, last accessed March 24, 2014.

16

17 Bertrand, C., M. F. Loutre, and A. Berger (2002), High frequency variations of the Earth’s  
18 orbital parameters and climate change, *Geophys. Res. Lett.*, 29(18),  
19 1893,10.1029/2002GL015622, 2002.

20

21 Bradley, R.S. (2014) *Paleoclimatology, Third Edition: Reconstructing Climates of the*  
22 *Quaternary*, Academic Press/Elsevier.

23

24 Bretagnon P. (1982), Theorie du mouvement de l’ensemble des planetes. Solution VSOP82,  
25 *Astron. Astrophys.*, 30, 141–154, 1982.

26

1 Chen, G. S., Kutzbach, J. E., Gallimore, R., & Liu, Z. (2011), Calendar effect on phase study  
2 in paleoclimate transient simulation with orbital forcing, *Climate dynamics*, 37(9-10), 1949-  
3 1960.

4

5 Falkowski, Paul G., Miriam E. Katz, Allen J. Milligan, Katja Fennel, Benjamin S. Cramer,  
6 Marie Pierre Aubry, Robert A. Berner, Michael J. Novacek, and Warren M. Zapol (2005),  
7 The rise of oxygen over the past 205 million years and the evolution of large placental  
8 mammals, *Science* 309, no. 5744 (2005): 2202-2204.

9

10 Falkowski, P. G., & Godfrey, L. V. (2008a), Electrons, life and the evolution of Earth's  
11 oxygen cycle. *Philosophical Transactions of the Royal Society B: Biological Sciences*,  
12 363(1504), 2705-2716.

13

14 Falkowski, P. G., & Isozaki, Y. (2008b), Geology. The story of O<sub>2</sub>. *Science*, 322(5901), 540-  
15 542.

16

17 Fröhlich, C. (2013)., Solar Constant: Construction of a Composite Total Solar Irradiance  
18 (TSI) Time Series from 1978 to present, Physikalisch-Meteorologisches Observatorium  
19 Davos, World Radiation Center,  
20 <http://www.pmodwrc.ch/pmod.php?topic=tsi/composite/SolarConstant>, last accessed Sept. 20,  
21 2013.

22

23 Hansen, J., Sato, M., & Ruedy, R. (2013), Global Temperature Update Through 2012. NASA  
24 ([http://www.nasa.gov/pdf/719139main\\_2012\\_GISTEMP\\_summary.pdf](http://www.nasa.gov/pdf/719139main_2012_GISTEMP_summary.pdf)), last accessed March  
25 24, 2014.

26

27 Hays, J. D. , J. Imbrie and N. J. Shackleton (1976), Variations in the Earth's Orbit: Pacemaker  
28 of the Ice Ages, *Science*: 194 (4270), 1121-1132. DOI:10.1126/science.194.4270.1121.

29

1 Huybers, P. (2006). Early Pleistocene glacial cycles and the integrated summer insolation  
2 forcing. *Science*, 313(5786), 508-511. Data and code posted at:  
3 <http://www.ncdc.noaa.gov/paleo/pubs/huybers2006b/huybers2006b.html>, last accessed  
4 September 24, 2013.

5

6 Huybers, P., & Denton, G. (2008), Antarctic temperature at orbital timescales controlled by  
7 local summer duration, *Nature Geoscience*, 1(11), 787-792.

8

9 Imbrie, J., E. A. Boyle, S. C. Clemens, A. Duffy, W. R. Howard, G. Kukla, J. Kutzbach, D. G.  
10 Martinson, A. McIntyre, A. C. Mix, B. Molfino, J. J. Morley, L. C. Peterson, N. G. Pisias, W.  
11 L. Prell, M. E. Raymo, N. J. Shackleton, J. R. Toggweiler (1992), On the structure and origin  
12 of major glaciation cycles: 1. Linear responses to Milankovitch forcing, *Paleoceanography*,  
13 7(6), 701– 738.

14

15 Imbrie, J., A. Berger, E.A. Boyle,S.C. Clemens, A. Duffy, W.R. Howard, G. Kukla, J.  
16 Kutzbach,D. G. Martinson, A. McIntyre, A.C. Mix, B. Molfino, J.J. Morley, L.C. Peterson ,  
17 N.G. Pisias, W. L. Prell, M.E. Raymo, N.J. Shackleton , and J . R. Toggweiler (1993), On the  
18 structure and origin of major glaciation cycles 2. The 100,000-year cycle. *Paleoceanography*,  
19 8(6), 699-735.

20

21 IPCC, 2013: Summary for Policymakers. In: Climate Change 2013: The Physical Science  
22 Basis. Contribution of Working Group I to the Fifth Assessment Report of the  
23 Intergovernmental Panel on Climate Change [Stocker, T.F., D. Qin, G.-K. Plattner, M.  
24 Tignor, S.K. Allen, J. Boschung, A. Nauels, Y. Xia, V. Bex and P.M. Midgley (eds.)].  
25 Cambridge University Press, Cambridge, United Kingdom and New York, NY, USA.

26

27 Joussaume, S., and P. Braconnot (1997), Sensitivity of paleoclimate simulation results to  
28 season definitions, *J. Geophys. Res.*, 102(D2), 1943–1956, doi:10.1029/96JD01989.

29

1 Jouzel, J., et al. (2007a), EPICA Dome C Ice Core 800KYr Deuterium Data and Temperature  
2 Estimates. IGBP PAGES/World Data Center for Paleoclimatology Data Contribution Series #  
3 2007-091. NOAA/NCDC Paleoclimatology Program, Boulder CO, USA.

4

5 Jouzel, J., V. Masson-Delmotte, O. Cattani, G. Dreyfus, S. Falourd, G. Hoffmann, B. Minster,  
6 J. Nouet, J.M. Barnola, J. Chappellaz, H. Fischer, J.C. Gallet, S. Johnsen, M. Leuenberger, L.  
7 Loulergue, D. Luethi, H. Oerter, F. Parrenin, G. Raisbeck, D. Raynaud, A. Schilt, J.  
8 Schwander, E. Selmo, R. Souchez, R. Spahni, B. Stauffer, J.P. Steffensen, B. Stenni, T.F.  
9 Stocker, J.L. Tison, M. Werner, and E.W. Wolff (2007b), Orbital and Millennial Antarctic  
10 Climate Variability over the Past 800,000 Years, *Science*, Vol. 317, No. 5839, pp.793-797.

11

12 Kasting, J. F., Whitmire, D. P., & Reynolds, R. T. (1993), Habitable zones around main  
13 sequence stars, *Icarus*, 101(1), 108-128.

14

15 Kasting, J. (2010), *How to Find a Habitable Planet*. Princeton University Press.

16

17 Kopp, G., and J. L. Lean (2011), A new, lower value of total solar irradiance: Evidence and  
18 climate significance, *Geophys. Res. Lett.*, 38, L01706, doi:10.1029/2010GL045777

19

20 Kump, L. R., Kasting, J. F., & Crane, R. G. (2010), *The Earth System*, San Francisco:  
21 Prentice Hall.

22

23 Laskar, J. (1999), The limits of Earth orbital calculations for geological time-scale use.  
24 *Philosophical Transactions of the Royal Society of London. Series A: Mathematical, Physical*  
25 *and Engineering Sciences*, 357(1757), 1735-1759.

26

27 Laskar, J., P. Robutel, F. Joutel, M. Gastineau, A. C. M. Correia, and B. Levrard (2004), A  
28 Long-term Numerical Solution for the Insolation Quantities of the Earth, *Astronomy and*  
29 *Astrophysics* 428, no. 1: 261-85. doi:10.1051/0004-6361:20041335.

1

2 Laskar, J., Fienga, A., Gastineau, M., & Manche, H. (2011), La2010: A new orbital solution  
3 for the long term motion of the Earth. *arXiv preprint arXiv:1103.1084*.

4

5 Laskar, J. (2014), Astronomical Solutions for Earth Paleoclimates, Institut de mecanique  
6 celeste et de calcul des ephemerides,  
7 <https://www.imcce.fr/Equipes/ASD/insola/earth/earth.html>, last accessed March 24, 2014.

8

9 Lisiecki, L. E., and M. E. Raymo (2005), A Pliocene-Pleistocene stack of 57 globally  
10 distributed benthic  $\delta^{18}\text{O}$  records, *Paleoceanography*, 20, PA1003,  
11 doi:10.1029/2004PA001071.

12

13 Lisiecki, L. E., Raymo, M. E., & Curry, W. B. (2008), Atlantic overturning responses to Late  
14 Pleistocene climate forcings. *Nature*, 456(7218), 85-88.

15

16 Lisiecki, L. (2014), LR04 Benthic Stack, <http://www.lorraine-lisiecki.com/stack.html>, last  
17 accessed March 24, 2014.

18

19 Loutre, M. F., Paillard, D., Vimeux, F., & Cortijo, E. (2004), Does mean annual insolation  
20 have the potential to change the climate? *Earth and Planetary Science Letters*, 221(1), 1-14.

21

22 Lüthi, D., et al. (2008a), EPICA Dome C Ice Core 800KYr Carbon Dioxide Data. IGBP  
23 PAGES/World Data Center for Paleoclimatology Data Contribution Series # 2008-055.  
24 NOAA/NCDC Paleoclimatology Program, Boulder CO, USA.

25

26 Lüthi, D., M. Le Floch, B. Bereiter, T. Blunier, J.-M. Barnola, U. Siegenthaler, D. Raynaud, J.  
27 Jouzel, H. Fischer, K. Kawamura, and T.F. Stocker (2008b), High-resolution carbon dioxide  
28 concentration record 650,000-800,000 years before present, *Nature*, Vol. 453, pp. 379-382.  
29 doi:10.1038/nature06949

1

2 Kopp, G., and J. L. Lean (2011), A new, lower value of total solar irradiance: Evidence and  
3 climate significance, *Geophys. Res. Lett.*, 38, L01706, doi:10.1029/2010GL045777.

4

5 Meeus, Jean (1998), *Astronomical Algorithms*, Willmann-Bell, Richmond, VA.

6

7 Milankovitch, M. (1941), *Kanon der Erdbestrahlung und seine Anwendung aufdas*  
8 *Eiszeitenproblem*, 633 pp., Ed. Sp. Acad. Royale Serbe, Belgrade. (English translation Canon  
9 of Insolation and Ice Age Problem, Israel program for Scientific Translation; published for the  
10 U.S. Department of Commerce and the National Science Foundation).

11

12 Muller, R. A., & MacDonald, G. J. (1997), Glacial cycles and astronomical forcing. *Science*,  
13 277(5323), 215-218.

14

15 Paillard, D., L. Labeyrie and P. Yiou (1996), Macintosh program performs time-series  
16 analysis, *EOS Trans.*, AGU, 77: 379.

17

18 Paillard, D. (2014), AnalySeries pour MacOS, LSCE,  
19 <http://www.lsce.ipsl.fr/Phoceas/Page/index.php?id=3> ( last accessed March 17, 2014)

20

21 Rial, J.A. (1999), Pacemaking the Ice Ages by Frequency Modulation of Earth's Orbital  
22 Eccentricity, *Science*: 285 (5427), 564-568. DOI:10.1126/science.285.5427.564

23

24 Rubincam, D. P. (1994), Insolation in terms of Earth's orbital parameters. *Theoretical and*  
25 *applied climatology*, 48(4), 195-202.

26

1 Standish, E. M., Newhall, X. X., Williams, J. G., & Yeomans, D. K. (1992), Orbital  
2 ephemerides of the Sun, Moon, and planets. *Explanatory supplement to the astronomical*  
3 *almanac*, 279-323.

4

5 Sinnott, Roger W. (1985) *Sky and Telescope* (70), August 1985, p. 159.

6

7 Timm, O., A. Timmermann, A. Abe-Ouchi, F. Saito, and T. Segawa (2008), On the definition  
8 of seasons in paleoclimate simulations with orbital forcing, *Paleoceanography*, 23, PA2221,  
9 doi:10.1029/2007PA001461.

10

11 USNO (2013), Selected Astronomical Constants, 2013 in *The Astronomical Almanac Online*,  
12 US Naval Observatory, Washington, DC, <http://asa.usno.navy.mil/SecK/Constants.html>, last  
13 accessed Sept. 27, 2013.

14

15 Zachos, J., M. Pagani, L. Sloan, E. Thomas, and K. Billups, (2001), Trends, Rhythms, and  
16 Aberrations in Global Climate 65 Ma to Present, *Science*, Vol. 292, No. 5517, pp. 686-693,  
17 27 April 2001. DOI: 10.1126/science.1059412.

18

19 Zachos, J., et al. (2008), Cenozoic Global Deep-Sea Stable Isotope Data. IGBP  
20 PAGES/World Data Center for Paleoclimatology Data Contribution Series # 2008-098.  
21 NOAA/NCDC Paleoclimatology Program, Boulder, CO, USA,  
22 <http://www.ncdc.noaa.gov/paleo/metadata/noaa-ocean-8674.html>, last accessed March 24,  
23 2014.

24

1 **Tables**

2 **Table 1.** Summary of constant and variable model input parameters.

Symbol	Constant/Variable	Value	Units	Reference	Notes
<i>AU</i>	Astronomical unit	149.597870700	10 <sup>6</sup> km	USNO (2013)	constant
<i>a</i>	Semi-major axis	149.598261150	10 <sup>6</sup> km	Standish et al. (1992)	1.00000261 AU (constant)
<i>T</i>	Sidereal orbital period	365.256363	Days	Meeus (1998)	constant
<i>S<sub>o</sub></i>	TSI at 1 AU	1,366*	W m <sup>-2</sup>	Fröhlich (2013)	Also see Kopp and Lean (2011)
<i>e</i>	Eccentricity	0.01670236**	--	La2004***	--
<i>ε</i>	Obliquity	23.4393**	degrees	La2004	--
<i>ω̃</i>	Longitude of perihelion	102.9179**	degrees	La2004	--

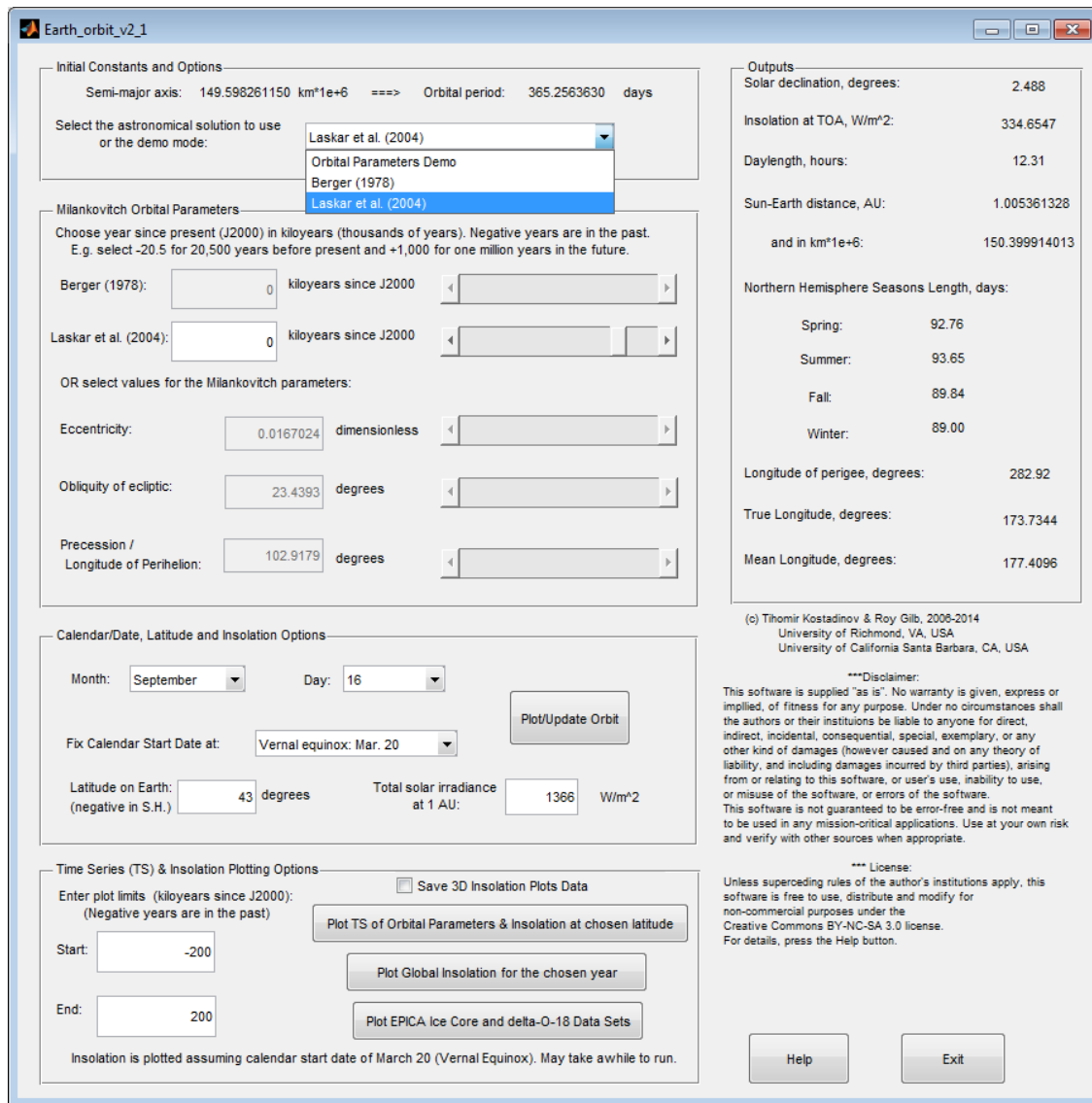
3 \*Users can change this default value.

4 \*\*Default J2000 values. Users can change these variables independently of each other or  
5 choose real astronomical solutions depending on the mode selected.

6 \*\*\*La2004 refers to Laskar et al. (2004)

7

# 1 Figures



2

3 **Figure 1.** Main MATLAB® GUI window of Earth Orbit v2.1. Input and output displayed  
4 corresponds to the graphical output of Fig. 2A, i.e. contemporary (J2000) La2004  
5 configuration for September 16, at 43° N latitude.

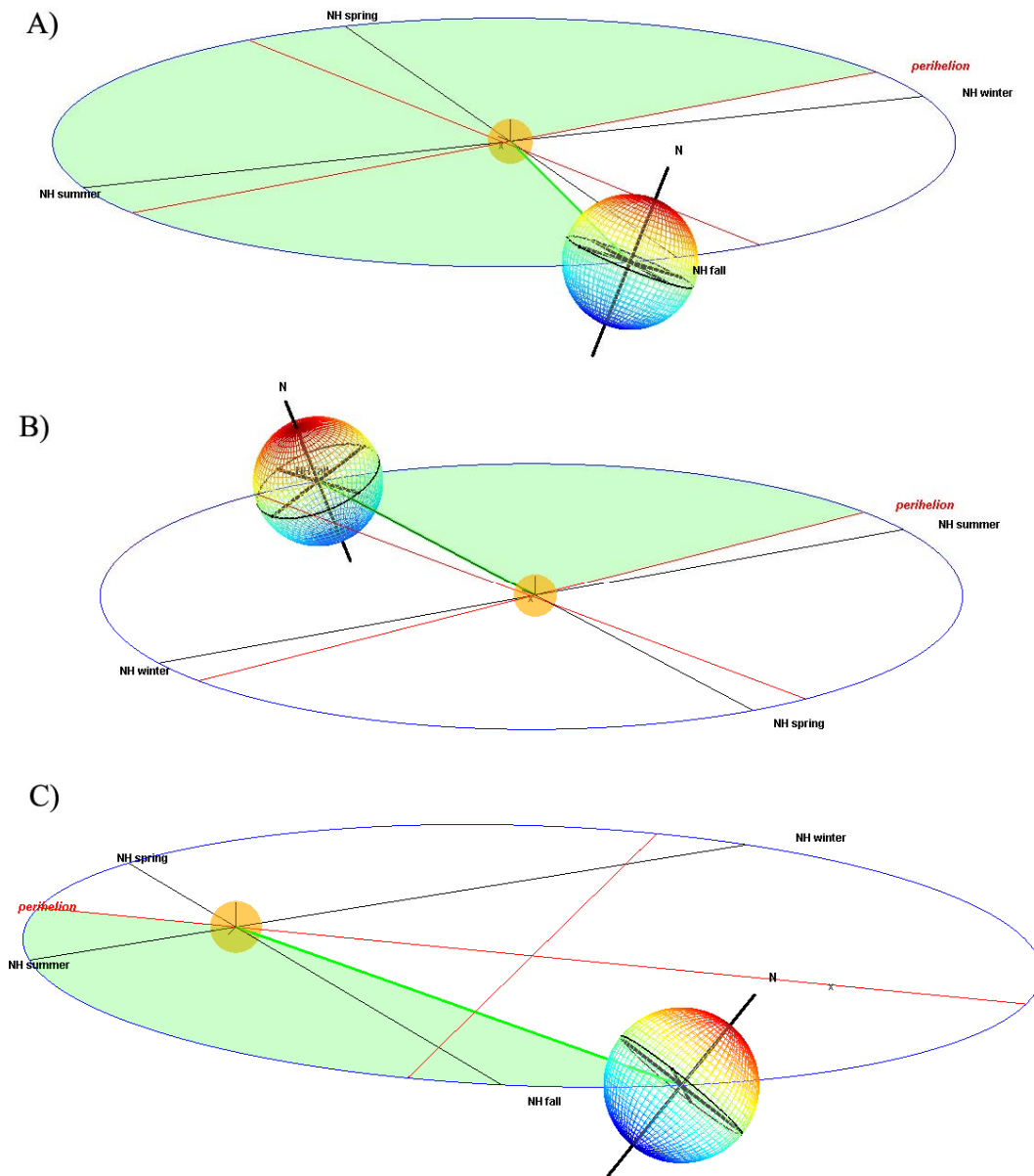
6

7

8

9

10



1

2 **Figure 2.** A) Present (J2000) orbital configuration for September 16, using the La2004  
 3 solution and the calendar start date fixed at vernal equinox on March 20. The orbital ellipse is  
 4 shown in blue, the semi-major and semi-minor axes (perpendicular to each other) are in red  
 5 and the lines connecting the solstices and equinoxes (also perpendicular to each other) are  
 6 shown in black. The perihelion point, as well as the equinoxes and solstices are labeled. The  
 7 Sun is shown as a semi-transparent yellowish sphere centered at one of the orbital ellipse's  
 8 foci, both of which are marked with an 'x' along the semi-major axis. The Earth is plotted  
 9 with its center on the corresponding place along the orbit, and the angle it has swept since last  
 10 perihelion passage (the true anomaly angle) is filled in semi-transparent light green. Earth's

1 Equator is plotted as a solid black line, as is its axis of rotation, with the North Pole marked.  
2 The spheres of the Earth and the Sun are not to scale, the rest of the figure is  
3 geometrically/astronomically accurate and to scale. This plot is in 3D and has pan-tilt-zoom  
4 capability in the Earth Orbit v2.1 model. The corresponding GUI with numerical ancillary  
5 output is shown in Fig. 1 (for latitude  $43^\circ$  N and  $S_o = 1,366 \text{ W m}^{-2}$ ). B) Real orbital  
6 configuration for September 16, 10 kyr in the future, using the La2004 solution and a March  
7 20 equinox as calendar start date; and C) demo (imaginary) orbital configuration for July 1  
8 (Vernal equinox fixed at March 20), Eccentricity = 0.6, Obliquity =  $45^\circ$ , Longitude of  
9 perihelion=  $225^\circ$ . The geometry is consistent with Berger et al. (2010), their Fig. 1, although  
10 it is being viewed in A) from the direction of fall equinox, as opposed to from the direction of  
11 spring equinox in their figure. The apparent eccentricity of the three orbits in Fig. 2 is also  
12 due to the view angle of the 3D plot and the respective projection onto a 2D monitor/paper;  
13 the intrinsic eccentricity can be judged by tilting the plot or observing the relative distance  
14 from the two foci (the Sun being at one of them) to the center of the ellipse, the intersection of  
15 the semi-major and semi-minor axes (red lines).

16

17

18

19

20

21

22

23

24

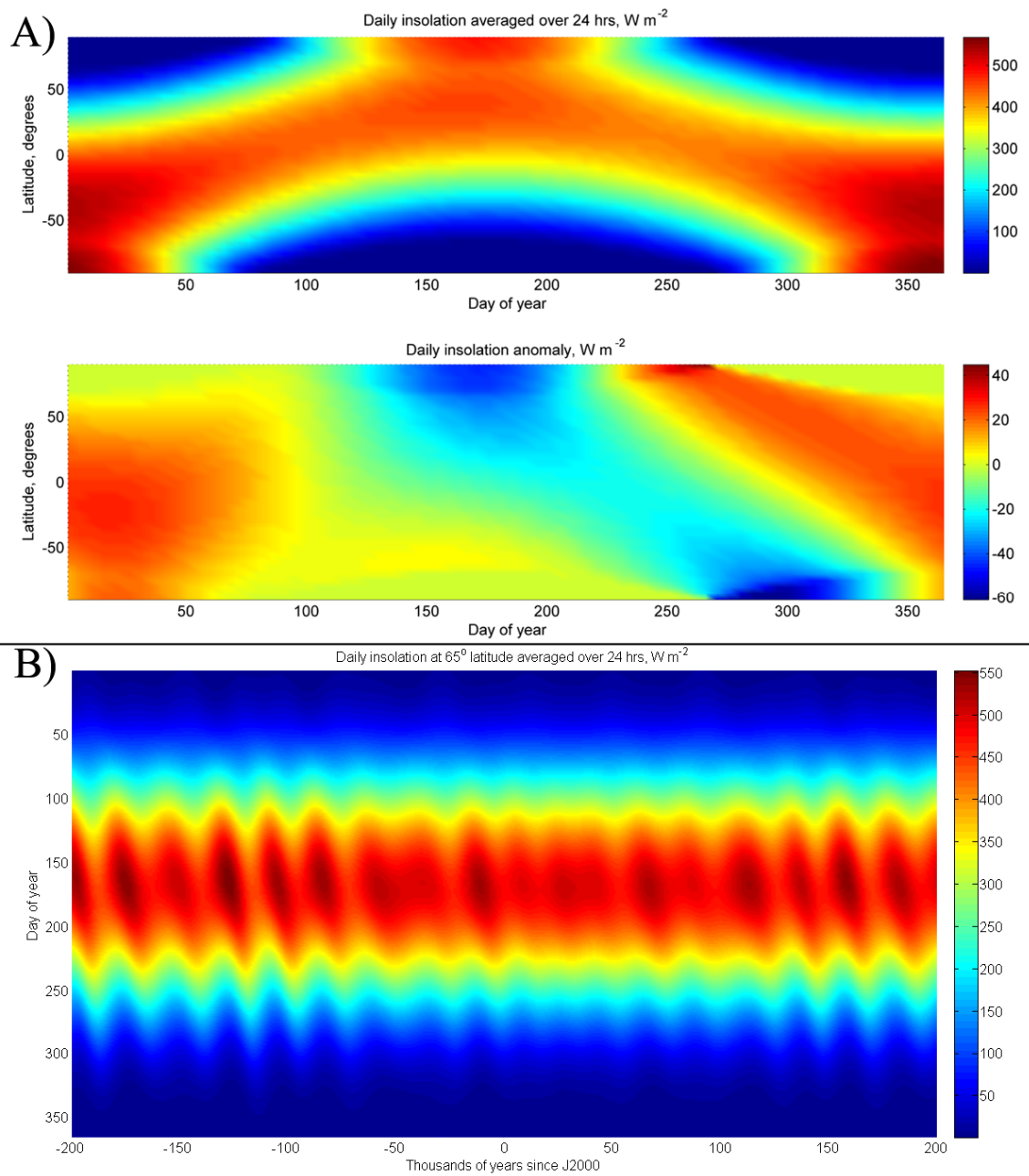
25

26

27

28

29



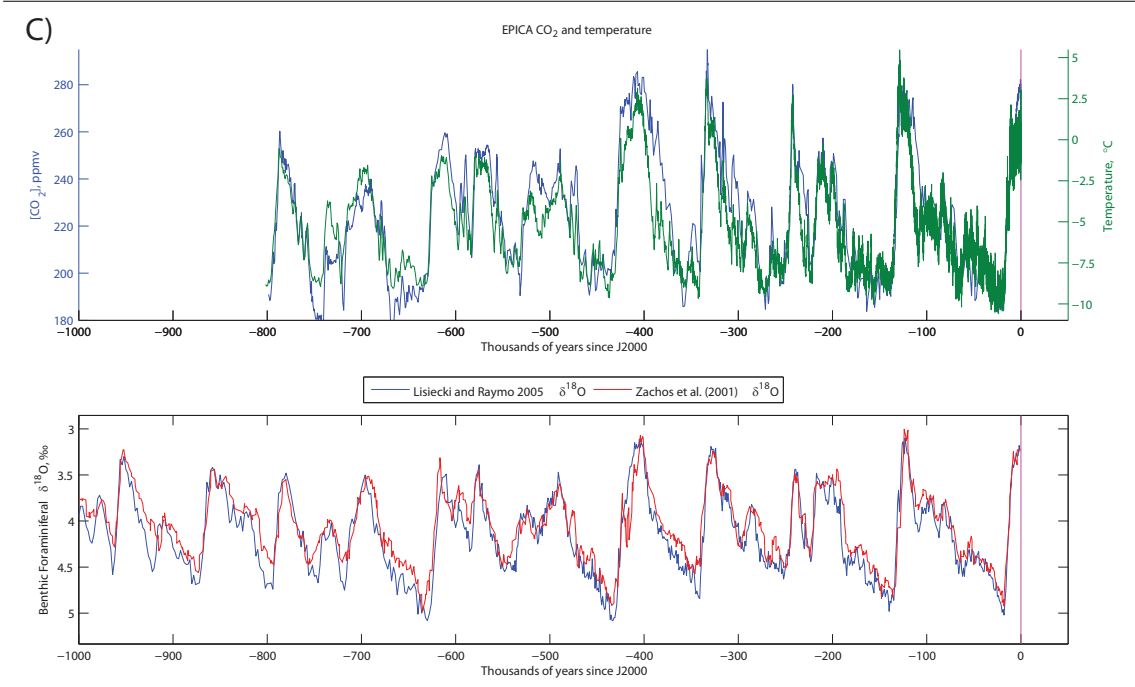
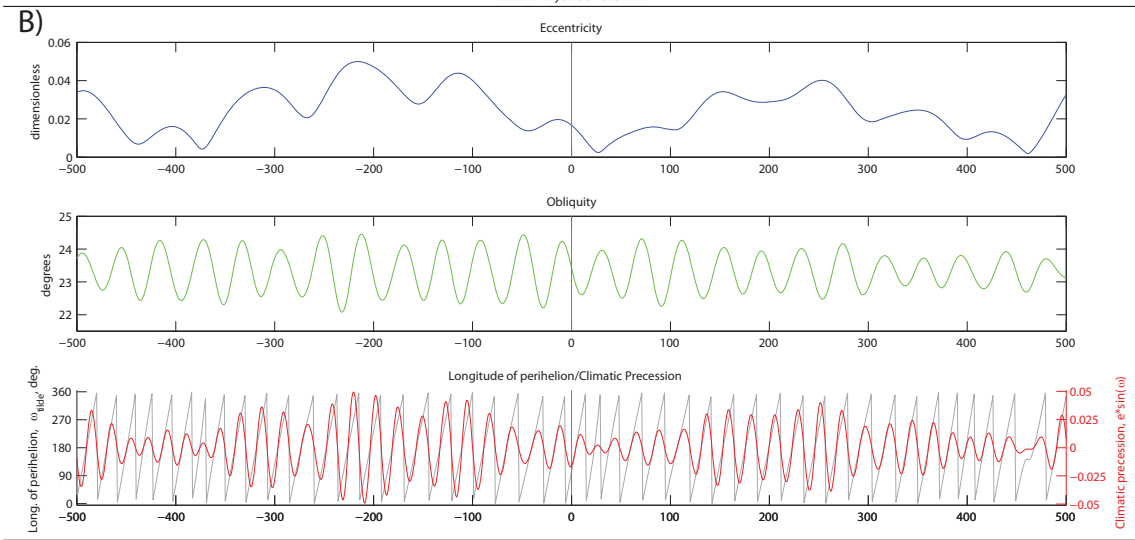
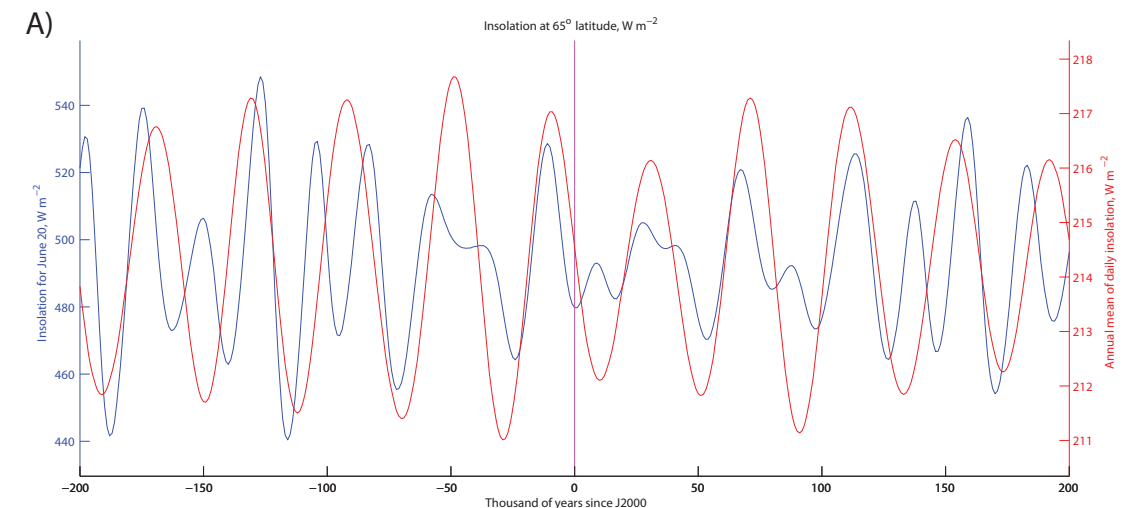
1

2 **Figure 3.** A) A day of year-latitude insolation plot for 115 kyr before present (J2000) (upper  
 3 panel) and the corresponding anomaly from J2000 (lower panel), using  $S_o = 1,366 \text{ W m}^{-2}$ . B)  
 4 Insolation time series at 65°N as a function of day of year, spanning 200 kyr before and after  
 5 present (J2000). Negative years are in the past.

6

7

8



1 **Figure 4.** A) Insolation time series plot spanning 200 kyr before and after present (J2000) at  
2 65° N on June 20th (blue) and annual average (red); B) Time series plots of Milankovitch  
3 orbital parameters spanning 500 kyr before and after present. Panels from top to bottom  
4 display eccentricity, obliquity, and longitude of perihelion and climatic precession; C) Time  
5 series plots of paleoclimatic data spanning one million years before and after present: EPICA  
6 ice core CO<sub>2</sub> and deuterium temperature (upper panel) and the Lisiecki and Raymo (2005)  
7 and Zachos et al (2001) compilations of benthic oxygen isotope ( $\delta^{18}\text{O}$ ) data (lower panel).  
8 Note the y-axis of the  $\delta^{18}\text{O}$  plot is inverted. Negative years for all Fig. 4 panels are in the past.

9

10

11

12

13

14

15

16

17

18

19

20

21

22

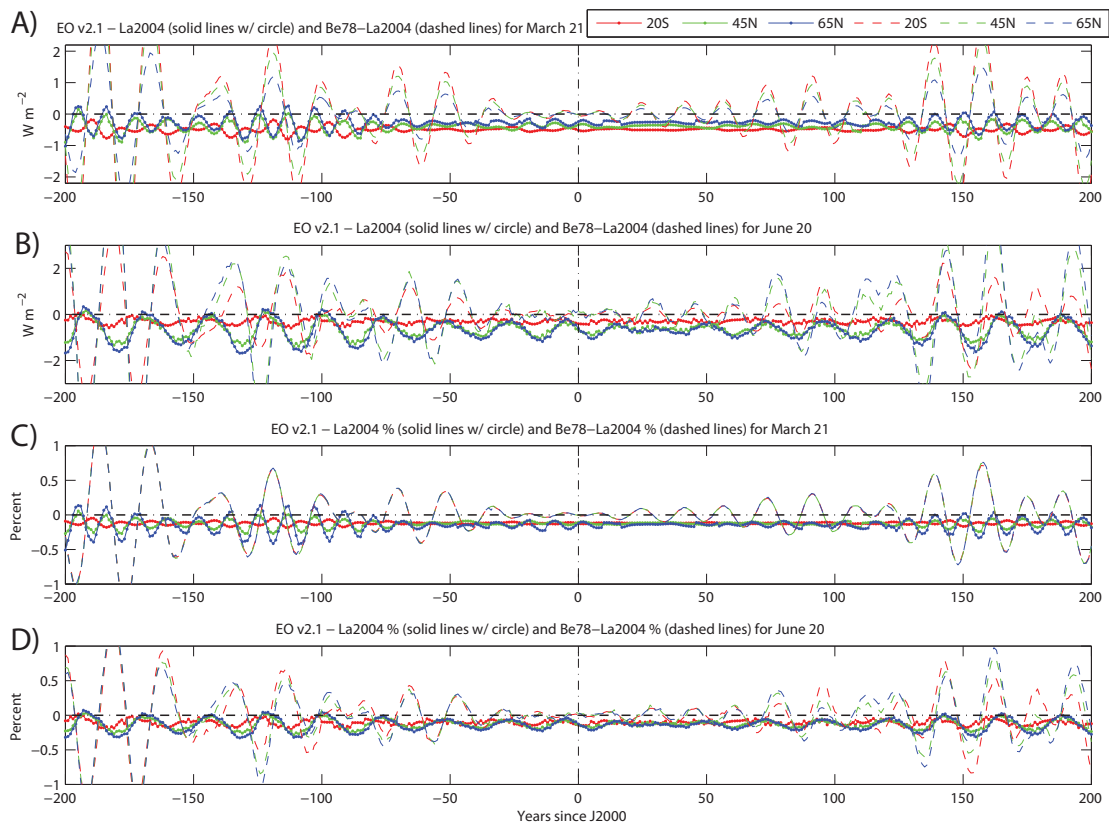
23

24

25

26

27



1

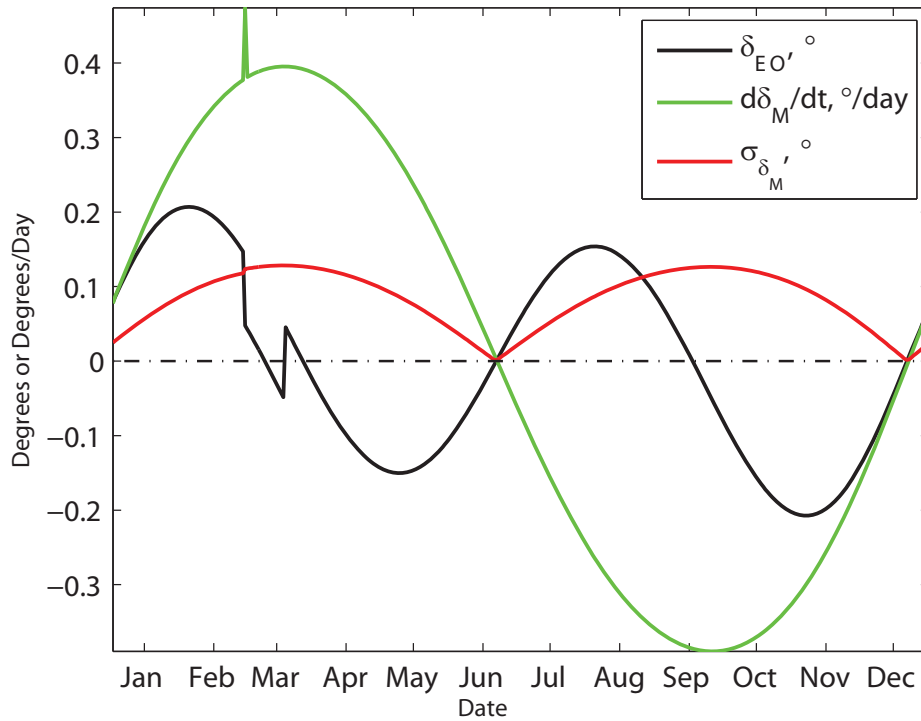
2 **Figure 5.** Absolute differences ( $\text{W m}^{-2}$ , solid lines with dots) between our insolation solution  
 3 (using the La2004 astronomical parameters) and the Laskar (2014) insolation solution (also  
 4 using the La2004 astronomical solutions; insolation provided by his Windows pre-compiled  
 5 package at <http://www.imcce.fr/Equipes/ASD/insola/earth/binaries/index.html>) for March 21  
 6 (A) and June 20 (B). Differences between the Be78 and La2004 astronomical solutions  
 7 (insolation for both computed by our model) are shown for comparison with dotted lines.  
 8 Data are shown for three different latitudes – 20 °S (red), 45 °N (green), and 65 °N (blue). C)  
 9 same as in A) but displaying percent insolation difference, D) same as in B) but displaying  
 10 percent insolation difference. Earth Orbit v2.1 insolation computations use the model’s own  
 11 orbital geometry with no additional *a-priori* input other than the Milankovitch parameter  
 12 solutions of La2004. Negative years are in the past. See Section 5.1 for details.

13

14

15

16



1

2 **Figure 6.** Solar declination validation: difference between solar declination as computed by  
 3 the internal geometry of the Earth orbit model and mean actual declination from the years  
 4 2009, 2010, 2011 and 2012 as computed for 12:00:00 UT for every day with the algorithms in  
 5 Meeus (1998) (black solid line). The rate of change of declination (green solid line) and the  
 6 standard deviation of declination for each date for the four years (red solid line,  $N = 4$  for  
 7 each data point) are also shown for reference. The model computations were performed with  
 8 the calendar start date fixed at vernal equinox of March 20. Feb. 29, 2012 was removed from  
 9 the analysis, so the abscissa corresponds to a given date, i.e. dates, not days of year were  
 10 averaged for a given mean solar declination across the four years. Abscissa ticks represent  
 11 the 15<sup>th</sup> of each month. If 0 UT is used for the Meeus computations instead, differences  
 12 (black curve) have a different pattern and are larger, but never exceed  $\sim 0.4$  degrees (not  
 13 shown). See Sect. 5.2 for details